Journal of
Marine Science and Engineering

MDPI

Article

Simulation of the Nearshore Sediment Transport Pattern and Beach Morphodynamics in the Semi-Enclosed Bay of Myrtos, Cephalonia Island, Ionian Sea

Alexandros Petropoulos [1,*], Vasilios Kapsimalis [2], Niki Evelpidou [1], Anna Karkani [1] and Katerina Giannikopoulou [1]

1 Faculty of Geology and Geoenvironment, National and Kapodistrian University of Athens, Panepistimiopolis, 15784 Athens, Greece; evelpidou@geol.uoa.gr (N.E.); ekarkani@geol.uoa.gr (A.K.); katagiann@geol.uoa.gr (K.G.)

2 Institute of Oceanography, Hellenic Centre for Marine Research, P.O. Box 712, 19013 Anavyssos, Greece; kapsim@hcmr.gr

* Correspondence: alexpetrop@geol.uoa.gr

check for updates

Citation: Petropoulos, A.; Kapsimalis, V.; Evelpidou, N.; Karkani, A.; Giannikopoulou, K. Simulation of the Nearshore Sediment Transport Pattern and Beach Morphodynamics in the Semi-Enclosed Bay of Myrtos, Cephalonia Island, Ionian Sea. *J. Mar. Sci. Eng.* **2022**, *10*, 1015. https://doi.org/10.3390/jmse10081015

Academic Editors: Harshinie Karunarathna, Markes E. Johnson, George Kontakiotis, Assimina Antonarakou and Dmitry A. Ruban

Received: 4 April 2022
Accepted: 20 July 2022
Published: 25 July 2022

Abstract: Myrtos Beach (Cephalonia Island, Ionian Sea, Greece) represents a pocket beach with strong touristic, economic and natural interest. In this research, the morphodynamic behavior of the coastal area (e.g., hydrodynamic and sedimentary state, morphology, orientation, etc.), the current wave conditions (extreme and dominant waves, wave exposure), and also external factors, such as human impact and the geotechnical condition of the wider area, are examined. Short- and medium-to-long-term analysis took place, such as mapping, sediment analysis, wave/wind analysis, numerical modeling, and satellite monitoring, in order to identify the dynamic forcing parameters related to geomorphology, sedimentology, and hydrology that prevail in the area. Additionally, the intense tectonics, the karstified limestones, and the steep slopes of the cliffs in combination with the frequent seismic events on the island set up a geotechnically unstable area, which often cause landslides on the beach of Myrtos; these supply the beach with a large amount of aggregates, constituting the main sediment supply. Wave exposure forcing conditions, longshore–rip current direction, and other hydrodynamic processes are stable with high values in the area, causing notable sediment transport within the bay boundaries. As a result, at Myrtos Bay there is a dynamic balance of the natural system, which is directly affected by human interventions. Taking also into consideration that Myrtos is one of the most famous beaches in Greece and one of the main attractions of Cephalonia Island with thousands of visitors every year, beach management must be focused on preserving the natural system of the coastal area.

Keywords: pocket beach; sand transport; longshore–rip current; hydrodynamic and sedimentary modeling; beach rotation; shoreline displacement

1. Introduction

A pocket beach is defined as a limited beach that is laterally bounded by two headlands [1–5]. The headlands significantly inhibit the sediment transport of nearby areas, restricting any hydrosedimentary processes between their boundaries and making them an autonomous and independent ecosystem, ideal for investigating beach morphodynamics [3,6–11]. Hydrodynamic conditions (longshore and rip currents, etc.) and beach characteristics (slope, grain size, nearshore bars, etc.) determine the morphological behavior of pocket beaches, which present a different circulation pattern than open water beaches [6,7,12–14]. An area with high wave exposure and increased wave radiation stress leads to coastal erosion in the exposed part and aggression in the sheltered part [7], making the determination of nearshore circulation (e.g., rip currents and longshore currents) and sediment transport trends important. Hence, pocket beaches are characterized as areas of limited sediment supply or as closed systems with restricted sediment exchange between them [3,15]. Under the worst-case scenarios, pocket beaches can lose significant volumes of sediment (temporarily or even permanently) if the sediment is transported outside the closure depth, which threatens their existence, posing significant risks landwards [16] (e.g., landslides and inundations). New sediment input can also occur through nearshore sediment sources [17], such as erosion of the backshore [18] (e.g., cliff and dunes) or input from local streams during stormy periods [19]. It is obvious that pocket beaches are particularly important areas for the ecosystem and the local tourism economy, yet, they are extremely sensitive to any change in existing conditions; therefore, their vulnerability to any dynamic change is of great significance at a global level [1,12,16,20,21]. Human activities are often the reason for the disruption of the coastal system, such as through civil engineering structures (e.g., river dredging, river damming and armoring, and anchored steel meshes) [22]. These factors reduce the available sediment that is naturally deposited in the coastal area, determining the inception of the erosion state.

The study of pocket beaches provides useful information on the prevailing pattern of nearshore sediment transport during different environmental conditions and its impact on beach evolution, but also regarding beach management [23]. Beach orientation, sediment classification, morphology, bottom composition, currents, and prevailing wind-generated waves are the main parameters for the morphodynamic variability that acts along and across the shore. The identification of the equilibrium in the beach planform could be characterized as static equilibrium, dynamic equilibrium, or unstable or natural reshaping [24]. Such parameters can help to determine the wave effect on sediment transport, to determine the duration of wave action, and to identify if there is a potential threat to the wider area.

In the present work, by identifying these processes, we aim to specify the coastal system formation of a pocket beach and to understand the nearshore hydrodynamics by analyzing the impact of the geomorphological parameters and the induced variability on circulation patterns. Numerical modeling with the MIKE 21 Flow Model (HD, SW, ST, and Shoreline Morphology modules) in addition to extensive subaerial and subaqueous field work and laboratory analysis may give promising predictions of beach evolution [25,26]. The ultimate goal of our work is to assess the dynamic balance of the natural system of the coastal area in a sustainable manner. Quantitative and qualitative results of sediment transport, and morphodynamic and hydrosedimentary results are presented alongside representative/extreme wave model simulations that were taken into account for the coast of Myrtos.

Myrtos Beach is a unique national monument of nature with high touristic and economic value, visited every year by thousands of tourists, and thus offering significant benefits to the local community of Cephalonia Island. Any negative evolution in the coastal system, such as coastal erosion, has a negative social and economic impact on coastal areas that revolve around tourism. Through the results of our study, the competent authorities will be able to implement better long-term management in the specific area of significant economic importance and take preventive actions. Nature-based strategic management activities are carried out to ensure long-term success in almost all sectors (environmental, touristic, economic, social, etc.). They can achieve effective long-term management by focusing on the preservation of natural and cultural resources while promoting the economic contribution to local communities.

2. Geological and Geomorphological Setting

Cephalonia Island is in the Ionian Sea (Greece). Myrtos Bay is located at the northwestern part of the island, between the northern section of Mt. Aenos and the southern part of Erissos peninsula (Figure 1). The stratigraphy of the area consists of carbonate sequences, marl formations, and turbidite limestones [27]. The tectonism in the area is intense and is characterized by faults in the NE–SW and NW–SE direction. The reverse fault of Agia Efimia, with a NW–SE direction, crosses the northern part of the bay, presenting a strike-slip component, and is characterized by uplift and erosion. The fault of Agia

Efimia, along with other active faults with a NE–SW and NW–SE direction, cut across Myrtos Bay and form a geotechnically unstable area [28,29]. Therefore, limestones on the slopes of Myrtos are strongly fragmented and locally karstified, and in some places, they turn into tectonic lattice due to the intense tectonism from the fault; they are also covered by colluvial deposits that derive from the weathering of steep slopes and consist of sand, gravel, and irregular limestone fragments [30]. Frequent seismic sequences on the island and weathering processes often cause landslides and rock falls on the steep slopes of the cliffs, causing damages on the beach of Myrtos and at various points on the road network [28]. The occurrence of landslides forms scree landforms, which also supply a large amount of aggregates to the beach.

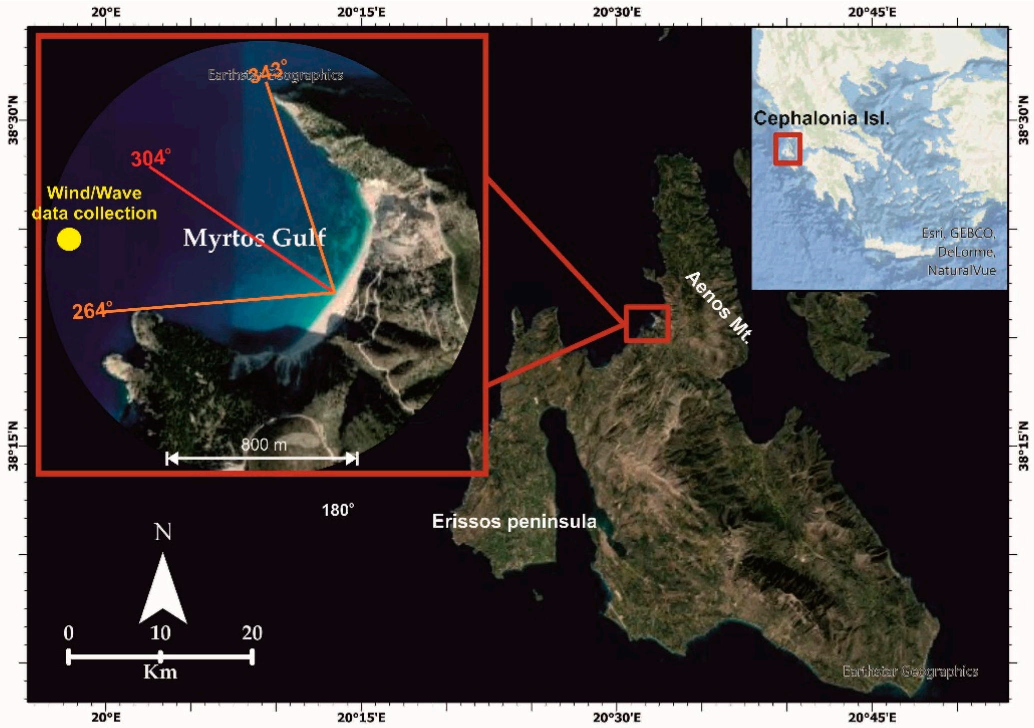

Figure 1. The island of Cephalonia located in the Ionian Sea. Myrtos Beach is located at the northwestern part of the island. The direction of Myrtos Bay ranges between 265 and 343°, whereas the orientation of the coastline is 304°.

The hydrographic network of the area is not well developed due to the karstic carbonate formations and the intense tectonics of the wider area. Independent and isolated seasonal streams of limited length and sediment supply flow in the bay; these streams are characterized by significant momentum during periods of heavy rainfall (flash floods), and deep erosion due to the steep slopes [28].

Geologically, the Myrtos area is part of the Pre-Apulian zone (external Hellinides, Paxos unit) and the lithological formations of which it is comprised are Upper Cretaceous limestone, Paleocene limestone, Eocene limestone, Miocene deposits, and Plio-Quaternary deposits (from the earliest to the latest). The approximate values that characterize the beach, considering its variability, are as follows: a length of 850 m, and a width of 100 m in the center and 30 m on both sides, whereas at the backshore a steep cliff of 30 to 300 m delimits the beach (Figure S1).

The direction of Myrtos Bay ranges between 265° and 343°, whereas the orientation of the coastline is 304° facing the NW, with a total width of 800 m from the entrance of the bay to the coast; it is bounded by two headlands preventing any sediment exchange with the neighboring coasts.

Based on the geographical position, the orientation of the bay, and the wind/wave data collection, resulting in the numerical reconstruction located at lat: 193,980.992 m/lon: 4,250,162.324 m (coordinates from Greek Grid) for Myrtos Bay for the period 1995–2004 [31], the coastline is mainly exposed to incoming waves from the N, NW, and W direction, with a fetch length extending to 266 km for the northwest direction, limited by the Apulian peninsula of Italy. The main annual wind intensity is classified between 3.3 and 7.9 m/s of the order of 3 to 4 Beaufort, with a frequency of ~13% and a NW direction. Extreme wind velocity values are also noticed from the same direction (10.7 to 19.3 m/s, 6 to 8 Beaufort) with a frequency of less than 2% [31]. Regarding the annual wave conditions, the most common wave approach direction to the beach is from the NW with a ~30% frequency, with prevailing waves of 0.5 to 1 m (~12.5% frequency). Extreme wave height values (2 to 5.2 m) also have a NW approach direction with a frequency of less than ~1.5% [31] (Figure S2).

3. Materials and Methods

The current coastal morphodynamic analysis was determined with two distinct approaches related to the duration. In situ field observations and measurements took place in October 2018 and March 2019, and allowed the short-term analysis of Myrtos Beach characteristics (e.g., topographic sections, sediment samples, bathymetric data, etc.), such as seasonal variations that change in short times. On the other hand, the medium-to-long-term analysis of the beach was accomplished using data on the wind and wave conditions for the period 1995–2017 [31–34] in order to identify the prevailing wave conditions and develop simulation scenarios. These scenarios were applied to the sediment and hydrodynamic transport numerical MIKE 21 Flow Model, which was coupled with the HD, SW, ST, and Shoreline Morphology modules in order to simulate the prevailing conditions through a dense array of measurements. Satellite images were also used (Google images from 2003 to 2019) to estimate the shoreline displacements through time. Medium-to-long-term analysis gives a sense how the coastal area has evolved over time and provides information on how it is likely to evolve in the near future (Figure 2).

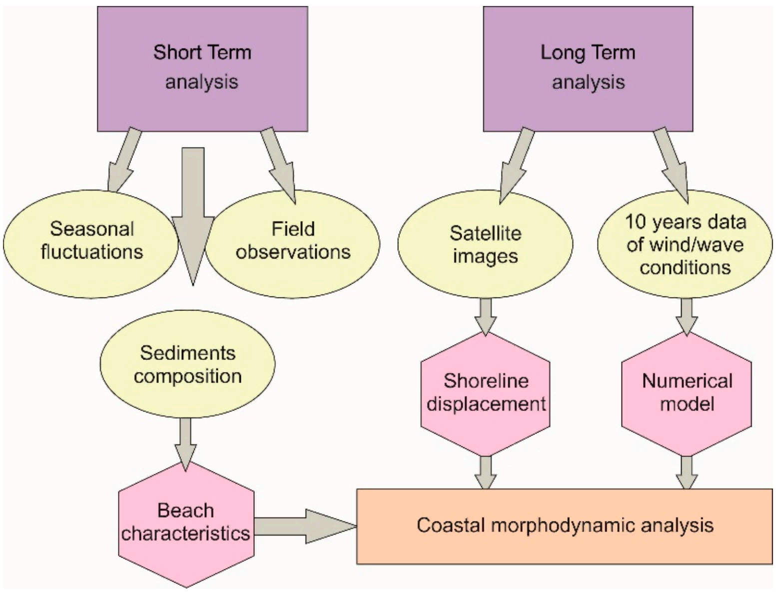

Figure 2. Flow chart that displays the methodology of the study area.

3.1. Short-Term Analysis and Measurements

In situ field surveys and measurements were carried out in two different periods, in October 2018 and March 2019, in order to estimate the representative characteristics of the beach in each season (summer/winter). Specifically, for each period the following were measured: (a) the evolution of seven sedimentary cross-shore profiles with 32 sediment samples (equally spaced in distance, ~80 m), (b) 55 topographic shore-sections at ~10 m distance and perpendicular to the coastline, which allowed a high resolution of the beach and c) recording of the coastline. A marine survey was also carried out, which included seabed morphological mapping of the bay, a bathymetric survey, and collection of 11 seabed sediment samples at a depth from 2 m to 15 m during each time period (Figure S3).

The elevation and geographical position were precisely determined byusing a Real-Time Kinematic (RTK) Differential Global Positioning System (DGPS). The detailed topo-bathymetric data were collected by the acquisition of side-scan sonar imagery (StarFish 450) and a single-beam echo sounder (Lowrance LCX-15MT). The substrate component mapping of the seabed was also performed with in situ field observations through a diving survey and underwater photography. The sediment samples for both periods were analyzed by dry granulometry and were sorted according to Folk and Ward's (1957) [35] nomenclature using the GRADISTAT (version 8.0) software by Simon J. Blott and Kenneth Pye (Royal Holloway University of London, UK) [36].

3.2. Medium-to-Long-Term Analysis

3.2.1. Digital Shoreline Analysis System (DSAS)

The comparison of the satellite images from 2003 to 2019 led to the quantification of the long-term shoreline displacements using the Digital Shoreline Analysis System (DSAS) application and the Net Shoreline Movement (NSM) tool in the ArcGIS (version 10.3) software by Esri (Redlands, California, U.S.) [37]. This tool offers the ability to calculate the distance between the oldest and the newest coastline and provides a value of the retreat or advance [38]. The satellite images were from the periods 06/2003, 12/2005, 01/2008, 04/2013, 07/2013, 03/2016, 04/2017, 10/2018, and 03/2019, and were selected because of their clearance at the land–water interface. They were georeferenced from WGS 84′ to WGS 84/UTM zone 34N. The National Cadastre was used as a reference base map, as it is a unified and constantly updated information system that records legal, technical, and other additional information on real estate and rights that are under the responsibility of the state.

3.2.2. Wind and Wave Data

The role of wind forcing is crucial for pocket beaches as, in most cases, it is the major forcing factor of wind-generated waves. The prevailing significant waves with high-energy flux, depending on their approaching direction, produce nearshore currents (longshore/rip current) that cause sediment transportation along the coast [39].

The wind and wave data for Myrtos Bay concern the period 1995–2017. The 10 years of data (1995–2004) are the result of the numerical reconstruction of wind and wave conditions [31] located at lat: 193,980.992 m/lon: 4,250,162.324 m (coordinates from Greek Grid). The wind regeneration data were derived from the atmospheric nonhydrostatic model SKIRON/ETA and the wave data from a combination of the above model with the WAM-Cycle 4 wave model [31]. The values of the quantities, since they derive from a numerical reconstruction, always involve a margin of error in relation to the actual wave and wind conditions. The wave data for 2005–2017 derive from the Copernicus Climate Change Service (ERA-Interim reanalysis dataset), providing a consistent European dataset for wave conditions that is produced by the ECMWF (European Centre for Medium-Range Weather Forecasts) [32–34].

3.2.3. Modeling

The numerical MIKE 21 Flow Model, coupled with the HD, SW, ST, and Shoreline Morphology modules, takes into account the space and time period of the prevailing and extreme conditions of the phenomena of interest by simulating the morphodynamics of an embayed beach with sediment transport and bed level changes due to currents or combined waves/currents. The MIKE 21 Flow Model has the efficiency to study the wave transformation over different temporal and spatial scales; it also allows repeating running tests with different wave exposure forcing conditions along different values of parameters [40] in order to better understand the nearshore circulation.

The numerical model estimates the coastal erosion processes and the natural variations in sand budgets, and allows for an assessment of marine spatial planning and the study of the impact and effectiveness of shore interference works. The reliable key calibration parameters, such as sediment grading, grain diameter, manning, and bed thickness, were calculated and used in the MIKE 21 Coupled Model FM simulations (Table 1) [41] in combination with bathymetry, sediment analysis, and substrate component data from the bay. The values of the main parameters used by the model were set based on the program manuals along with empirical validation through the repeated running of tests. The model was successfully applied and tested in a number of basic, idealized, realistic, and complicated situations from which the output results can be compared with analytical solutions or information from the literature [42–44].

Table 1. Main parameters of MIKE 21 Coupled Model FM used in simulations.

Parameters	Values
Sediment Grading ($\sqrt{}$(d_84 ÷ d_16))	1.1–2
Mean Grain Size (Mz)	0.07–1.9 mm
Manning Number	10–32 $m^{1/3}/s$
Bed Thickness	0.05–2 m

4. Results

The results of this work concern two distinct approaches, related to the in situ measurements and the statistical and numerical model results, which are presented below. The results from the topographic, sedimentological, and morphodynamic seasonal analysis of the subaerial part of the morphological profile sections reveal the difference between the two seasonal periods. Additionally, the statistical results of the DSAS-NSM from 2003 to 2019 allowed to identify the displacement of the coastline. Finally, the results from the MIKE 21 Coupled Model FM simulations examined the hydrodynamic and sediment transport for each scenario/situation.

4.1. Morphological and Nearshore Characteristics and Grain Size Analysis

The coastline length of Myrtos Beach is 860 m, with a limited width at both ends having an average value of 30 m, whereas the central part of the coastal width reaches 80 m. Vegetation is observed, during both periods, only at the central part of the coast, at the backshore area, and near the cliffs (~60 m from the coastline). Human impact is limited at the base of the cliff through the construction of a local road and a parking area, and also at the central area of the backshore with a human structure.

The sedimentary materials in both periods show some similarities in terms of grain distribution. Figure 3a,b depicts that, for marine sediments, the finest material is concentrated in the SW area, developing a long tongue of fine sediments (mud, sand) surrounded by hard substrate with coarse-grained sediments (granule, pebbles), whereas in the coastal area there is a difference in the grain distribution, as in summer the backshore and foreshore area consists mainly of fine sediments (sandy sediments) in contrast to the winter period, where the sediment distributed in the area is characterized as coarse (gravel).

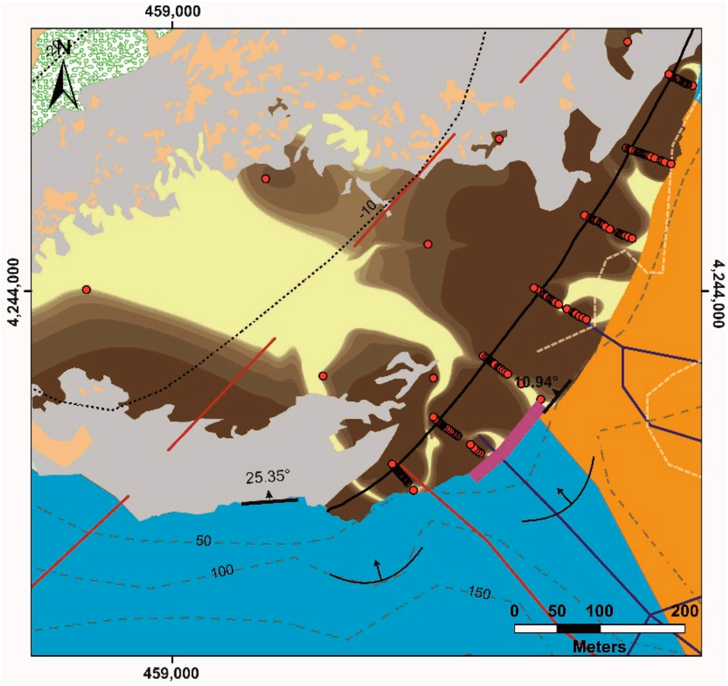

(a)

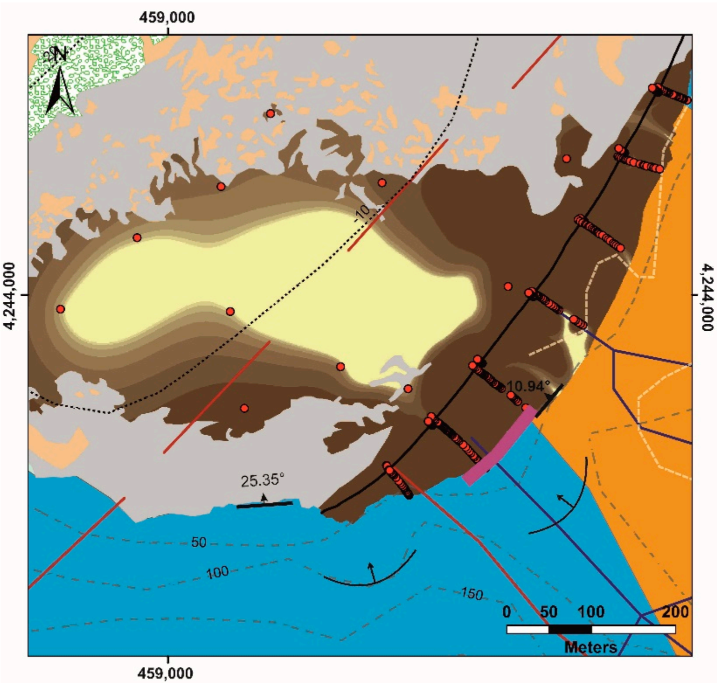

(b)

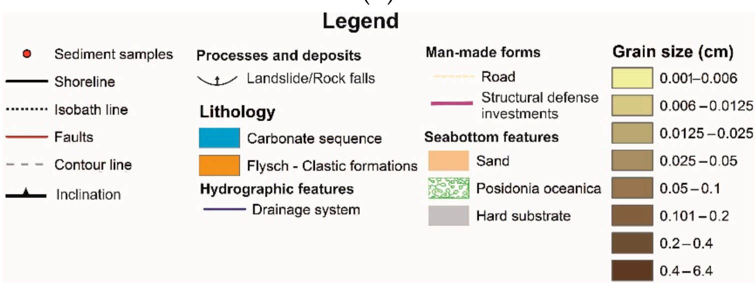

Figure 3. Grain size distribution in the summer–October 2018 (**a**) and winter–May 2019 (**b**) period.

Figure 4 depicts the temporal evolution of the beach profiles from October 2018 to May 2019, located from the backshore until the water breaker zone. Significant variability is present at the surf and swash zone where the seasonal fluctuation is clear, with sediment accumulation during the summer months and erosion during the winter months. The summer Beach Profile 3 displays the highest sediment supply compared to that of the winter period. The other beach profiles follow the same pattern (compared to the summer and winter profile) on a smaller scale. Additionally, morphological formations such as beach berms are formed along the beach in both periods, but in the winter months they are smaller and more in number in contrast to the summer months. Sediment composition in both periods is characterized as gravelly sand to coarse gravel, confirming that the sediment supplies is a combination derived from landslide materials off nearby cliffs and the coastal high-energy environment. The beach area is composed of different spatial and quantitative values, with the coarser sediments located landward and well sorted, whilst at the dynamic swash zone, different sizes of sediments are located and poorly sorted. Most fine sediments are absent due to high wave energy, whereas the coarser remains. The winter profiles are characterized by coarser sediments that are found mainly at the swash zone in contrast to the summer profiles.

Beach Profile 2 to Beach Profile 5 display a smoother profile with finer sediments than the rest of the beach profiles (BP 1, BP 6–7), especially during the summer period. Beach Profile 4 and 5 are the most exposed to the wave conditions, as topographic anomalies occur along their entire length.

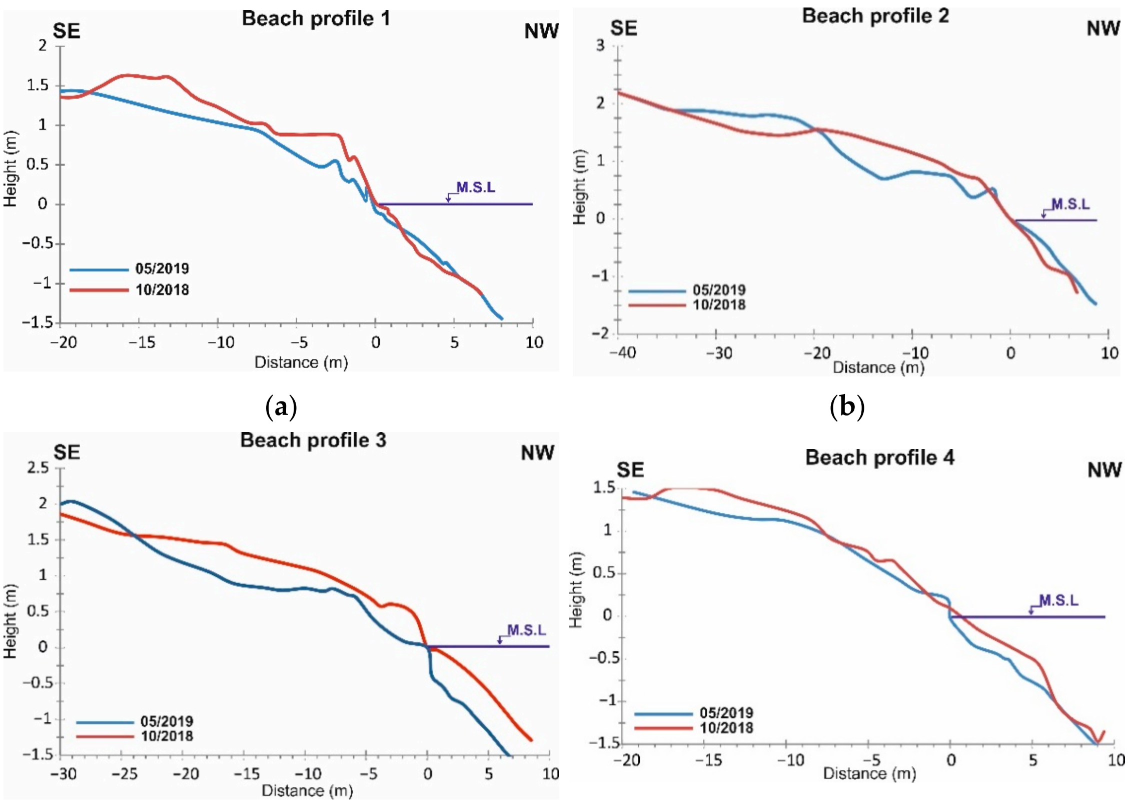

(**a**) (**b**)

(**c**) (**d**)

Figure 4. *Cont*.

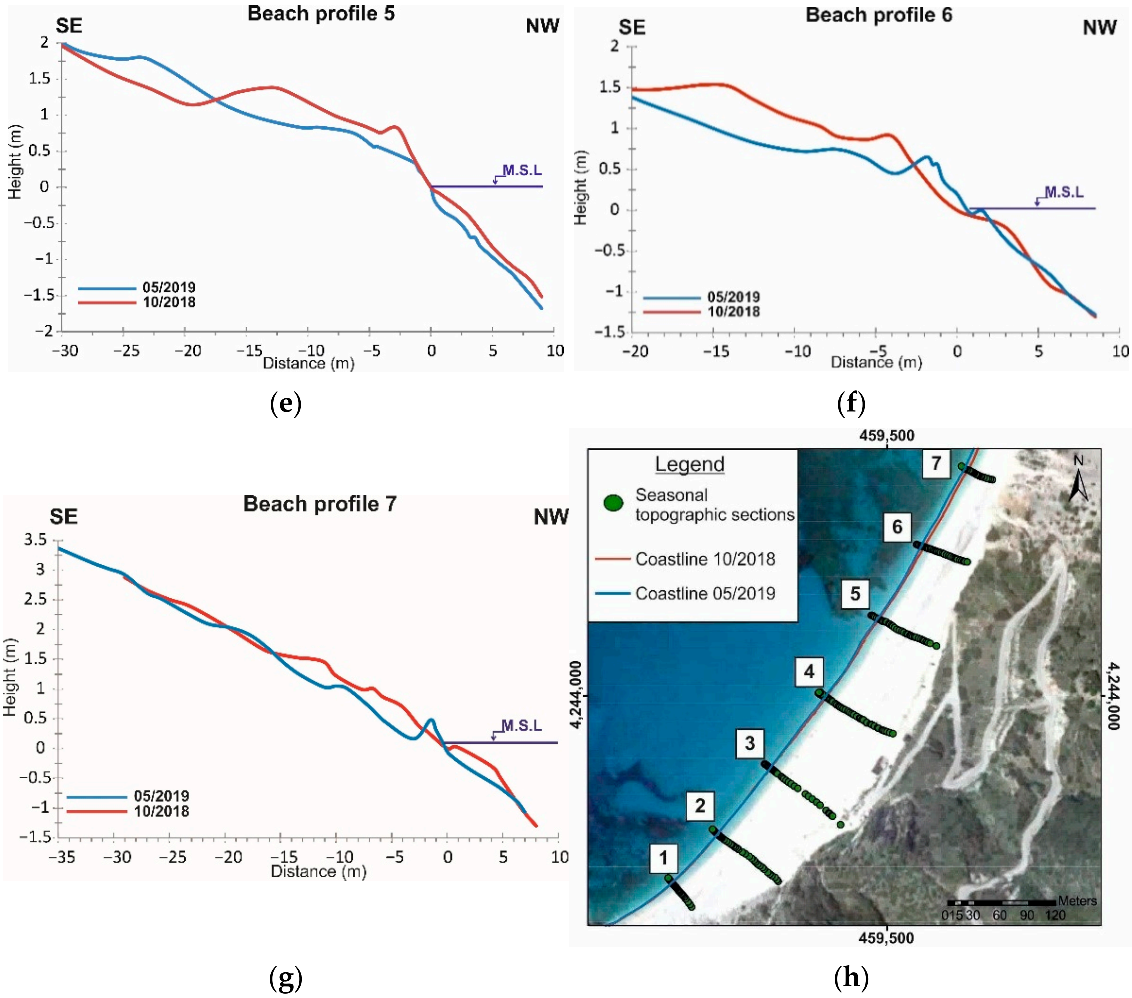

Figure 4. Seasonal evolution of beach profiles. (**a**–**g**) display the corresponding beach profile, focusing on the surf and swash zone. (**h**) specifies the geospatial location of the beach profiles sections.

Myrtos Bay presents a topographic anomaly in the slope at the bottom, as between the depths of 2 and 8 m the slope is steep (20 m from the coastline); then, until the depth of 20 m, the slope becomes relatively gentle, and up to a depth of 34 m it becomes steep again (Posidonia *Oceanica* meadow area). Afterwards, the seabed presents a variation of inclination from steeper to mild values. The closure depth is estimated at 10 m with a nearshore slope at 5°. The calculation of the closure depth is supported by the Hallermeier equation [45]. The maximum measured depth of the enclosed bay is 45 m and is located at the entrance of the bay. The bathymetric contours are parallel to the coastline from the entrance of the bay until the isobaths of 18 m, whereas from this area until the shoreline, the bay is divided into two parts. The first includes the SW area where the isobaths are parallel to the coastline, and the second, the NE area where the isobaths are affected by the hard substrate, creating a swallow environment (Figure 5a). The Myrtos pocket beach can be exposed to high wave energy due to the steeply sloping sea bottom near the coast.

Wave radiation stress is significant to detect the circulation pattern in the coastal area, where longshore and cross-shore currents act, especially at the surf zone. Wave radiation stress acts on mean flow, causing wave setup and wave-induced current [46]. Figure 6 shows the isobaths, the gradient spatial distribution, and the sea bottom composition, which specify the fluctuation of the radiation stress areas. At the central part of this area, the radiation stress is generally normal towards the coastline and reaches maximum when the bottom topography changes abruptly, as at the wave break zone, where the significant wave height changes most (hard substrate, isobaths of 8 m).

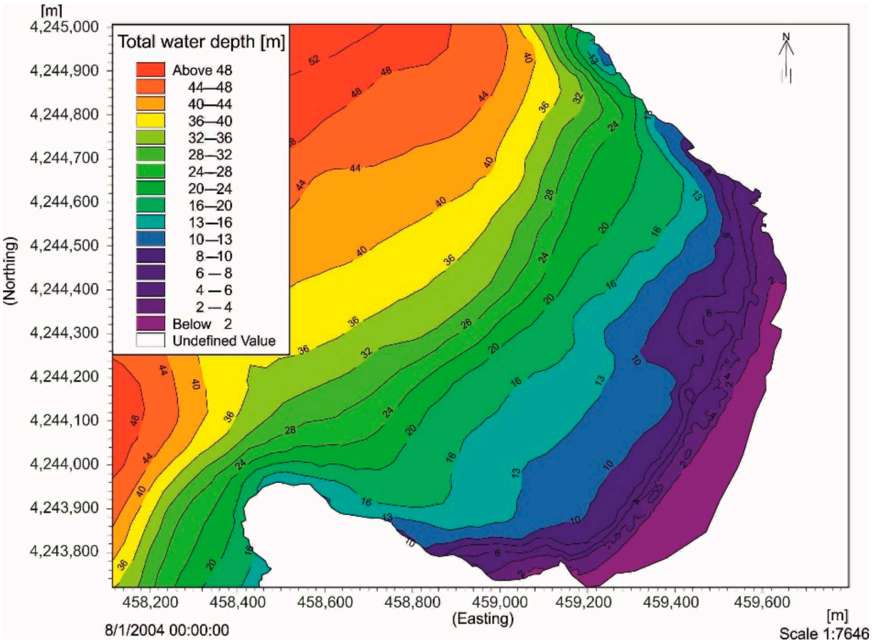

(**a**)

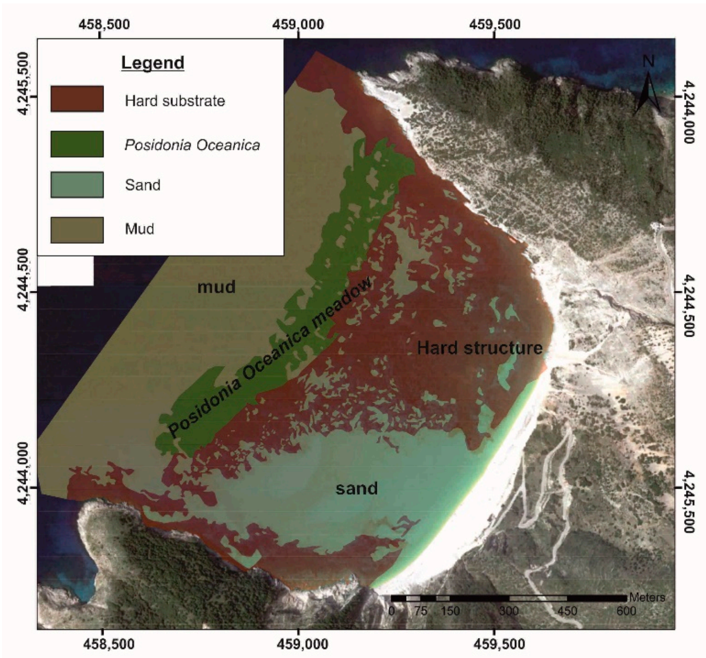

(**b**)

Figure 5. (**a**) Bathymetry map of Myrtos Bay, (**b**) substrate component mapping of the seabed of Myrtos Bay.

The total surface area of the bay is about 1 km^2 and the seafloor consists of noncohesive material (0.58 km^2), rocky outcrops (0.32 km^2), and a seagrass (Posidonia Oceanica) meadow (0.1 km^2). The sandy, gravelly, and hard substrate is located from the nearshore zone to a depth of 22 m. The meadow is developed at depths between 22 and 32 m, whereas the deepest part of the bay is covered by fine-grained sediment (mud) (Figure 5b).

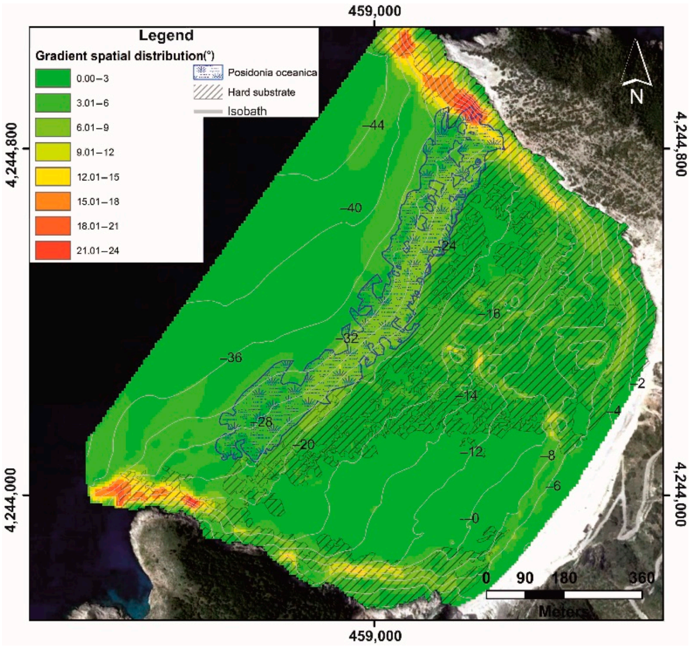

Figure 6. Gradient spatial distribution of the seabed of Myrtos Bay.

4.2. Digital Shoreline Analysis (DSAS)

The use of satellite images from 2003 to 2019, in combination with the DSAS-NSM (ArcMap) software tool, led to the quantification of the long-term shoreline displacements. The statistical results show that the earthquake event of 2014 [28,29,47–50] had a significant role in the evolution of the coast, as from 2003 to 2013 the average retreat of the shoreline reached 8 m for the central and southern part of the beach due to the limited sediment supply from the land, with an average regression rate of 1.3 m/year. In the northern part, sediment deposition results showed an average coastal advance of 4 m, as a result of the beach rotation mechanism. After the earthquake event and until 2019, the statistical results demonstrate that deposition phenomena prevailed in the area, with an average shoreline progradation of about 15 m (Figure 7). The shoreline progradation had an average rate of 1.4 m/year at both edges of the coast and 2.5 m in the central part of the beach.

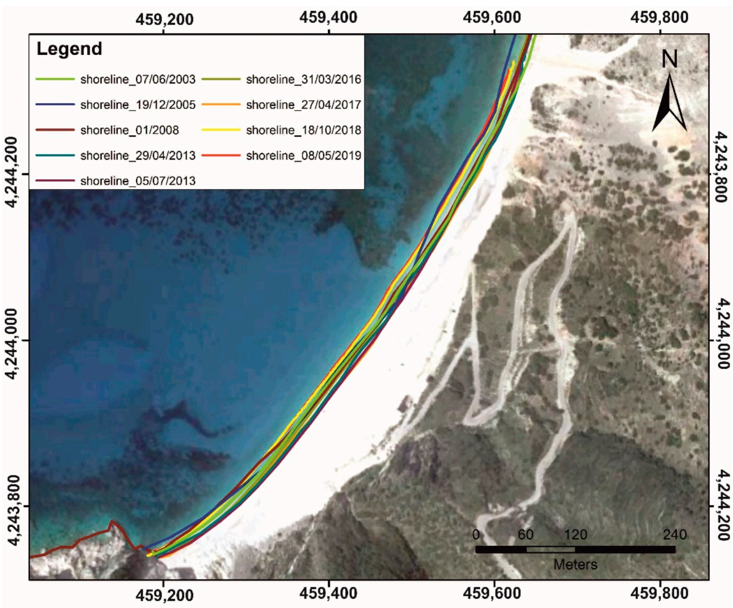

(**a**)

Figure 7. *Cont.*

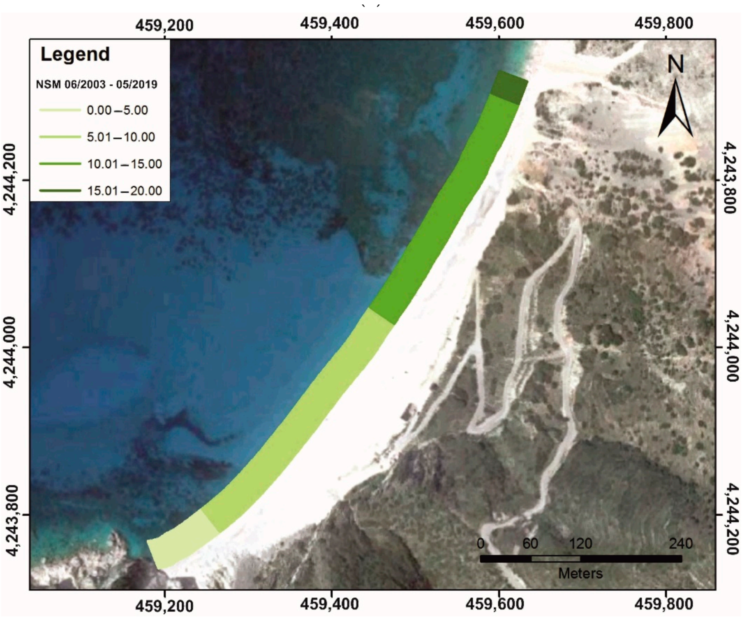

(**b**)

Figure 7. (**a**) Shoreline evolution. Nine different shoreline displacements for the period 2003 to 2019. (**b**) Net shoreline movement at Myrtos Beach. The figure displays the coastline fluctuation for the period 2003 to 2019.

The result for the seasonal displacement of the shoreline (10/2018–05/2019) reflects a stable situation with little variation between summer and winter, based mainly on the seasonal beach rotation mechanism.

4.3. Model Examination

The boundary conditions applied to the model were obtained from two directions, depending on the significant wave's direction and the orientation of the coastline, as the sediment transportation takes place in both directions. For each part of the coast, one scenario corresponds to the prevailing conditions, depending on their approaching direction, which contribute to the sediment transport from one side to the other, and the second scenario corresponds to the opposite direction. The prevailing conditions correspond to the representative significant waves for each scenario according to the maximum wave energy flux in each direction annually [41,51–55], estimating the potential and total sediment transport at the time of simulation. The direction of Myrtos Bay ranges between 265° and 343°, whereas the orientation of the coastline is 304°; a scenario for each direction of the coast was determined, estimating the pure and total sediment transport at the time of simulation (scenario 1: 264–304°, scenario 2: 305–343°) (Figure S4). The duration of each simulation scenario was determined from the total flow of wave energy at an annual frequency to the maximum energy flux (Table 2).

Table 2. Representative scenarios taken into account for Myrtos Bay.

Scenario	H Sign. (m)	T(s)	MWD (Deg N)	Duration (Days)
1	2.25	8.25	300	7
2	0.75	5.25	315	203

Additionally, notable is the sediment transport that takes place during extreme wave events. Taking into account the wind and wave data of the study area [31–34], the most extreme event was identified as occurring between the 265 and 343° direction [56] (Table 3).

Table 3. Extreme wave event taken into account for Myrtos Bay.

Scenario	Hmean (m)	Hmax (m)	Tmax (s)	MWD (Deg N)	Duration (Days)	Start Date—Time
Extreme Event	2.7	5.19	10.26	304	2.2	24/11/2001—00:00

Wave radiation stress is significant where the depth bottom decreases drastically, leading to an increase in wave energy dissipation through bottom friction and wave breaking, especially within the surf zone area, and a decrease in wave height.

The circulation patterns (longshore/cross-shore currents) for each wave radiation stress in the respective scenarios and each extreme wave event are the result of the contribution of wave breaking due to depth change, wave refraction, wave diffraction, and sea bottom component effects (Figures 5 and 6) [46]. The prevailing conditions corresponding to the annual representative waves from 265 to 304° were simulated for scenario 1, and they have a mean energy flux direction of 300°, significant wave height of 2.25 m, wave period of 8.25 s, and time of simulation of 7 days (Figure 8a). The coastal currents of the study area are characterized by an average velocity of 0.19 m/s and a maximum value of 1.09 m/s, located in the southern part of the coast and parallel to the coastline in a NE direction. It is worth noting the formation of two longshore currents parallel to the coastline, which are oriented from SW to NE and from NE to SW; they meet each other in the middle of the coastline, where they create a rip current with an average velocity of 0.11 m/s (maximum value 0.28 m/s), up to a depth of ~10 m, at a distance of 240 m from the coastline (Figure 8b). Sediment transportation and seabed variation values are directly affected by the way coastal currents act on the area. The first is oriented to the NE and the other to the SW, whereas they meet each other in the middle of the coastline, with a direction to the NW and to the deeper parts. The largest volumes of coastal sediment transportation occur along the coastline with values ranging between 1.1×10^{-6} and 5.7×10^{-4} m^3/sec/meter (average value 4×10^{-5} m^3/sec/meter). Affected by the coastal currents and the sediment transportation, seabed variation concerns the transport and deposition of sediments from the coast, and especially from the surf zone to the deeper parts (7 m), creating longshore bars at a distance of 60 m from the coastline, with a range of values between −2 m (surf/swash zone) and −3.4 m (breaker zone) (Figure 9).

Scenario 2 is characterized by a mean energy flux direction of 315°, significant wave height of 0.75 m, wave period of 5.25 s, and time of simulation of 203 days in order to simulate the prevailing conditions corresponding to the annual representative waves between 305 and 343°(Figure 10a). The energy flux that reaches the coast is significantly reduced compared to Scenario 1. Coastal currents have an average velocity of 0.06 m/s and a maximum value of 0.47 m/s in the southern part of the coast, perpendicular to it. A typical longshore current is formed at the northern part of the coast with an orientation to the SW, whereas at the southern part of the coast the currents act perpendicular to the coast (Figure 10b). The values of sediment transportation and seabed variations depend on coastal current values; sediment transportation takes place in two areas: (a) from north to south until the middle of the coast, with an average value of 1.3×10^{-5} m^3/sec/meter, and (b) perpendicular to the coast, in its southern part, with an average value of 1.9×10^{-5} m^3/sec/meter. The prevailing trend of seabed variation concerns the transport and deposition of sediments by displaying erosion at the northern part of the coast, with average values of −0.15 m, and deposition at the southern part with average values at 0.88 m. Maximum values of seabed variations are estimated as −1.96 m for the eroded area and 3.97 m for the deposition area (Figure 11).

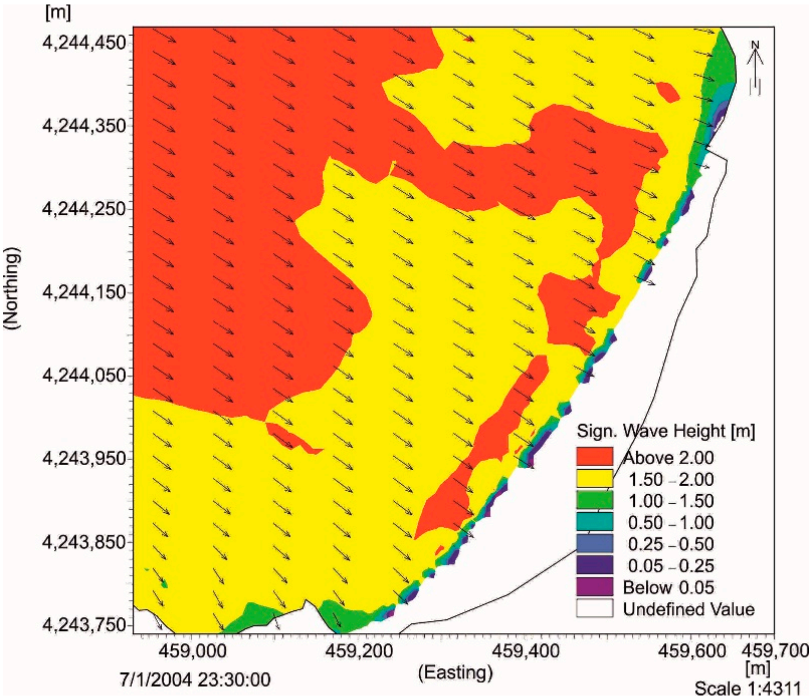

(**a**)

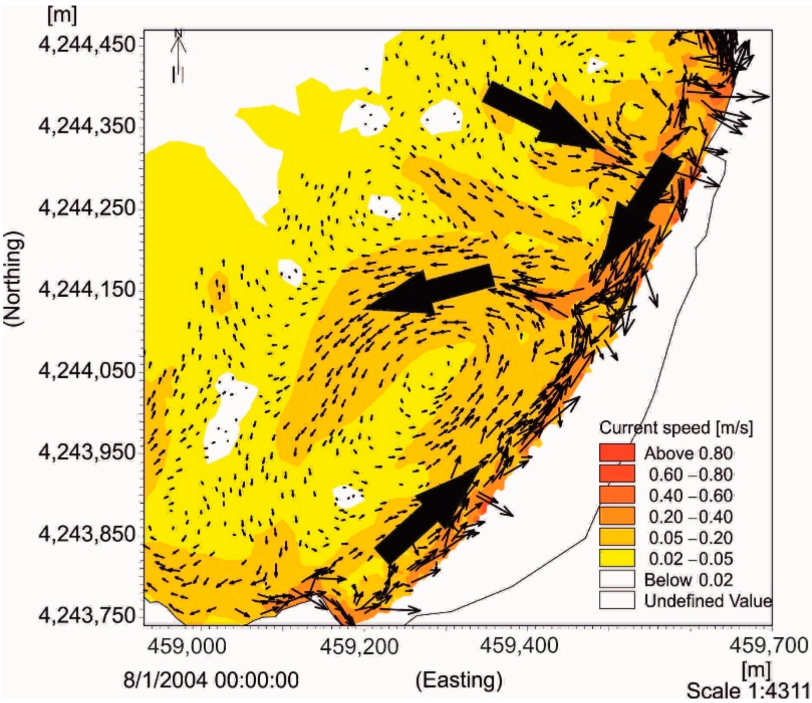

(**b**)

Figure 8. Model simulation for scenario 1. (**a**) Map of significant wave height distribution. (**b**) Map of coastal current velocity. The arrows show the pattern of behavior of the (**a**) Sign. wave and (**b**) current.

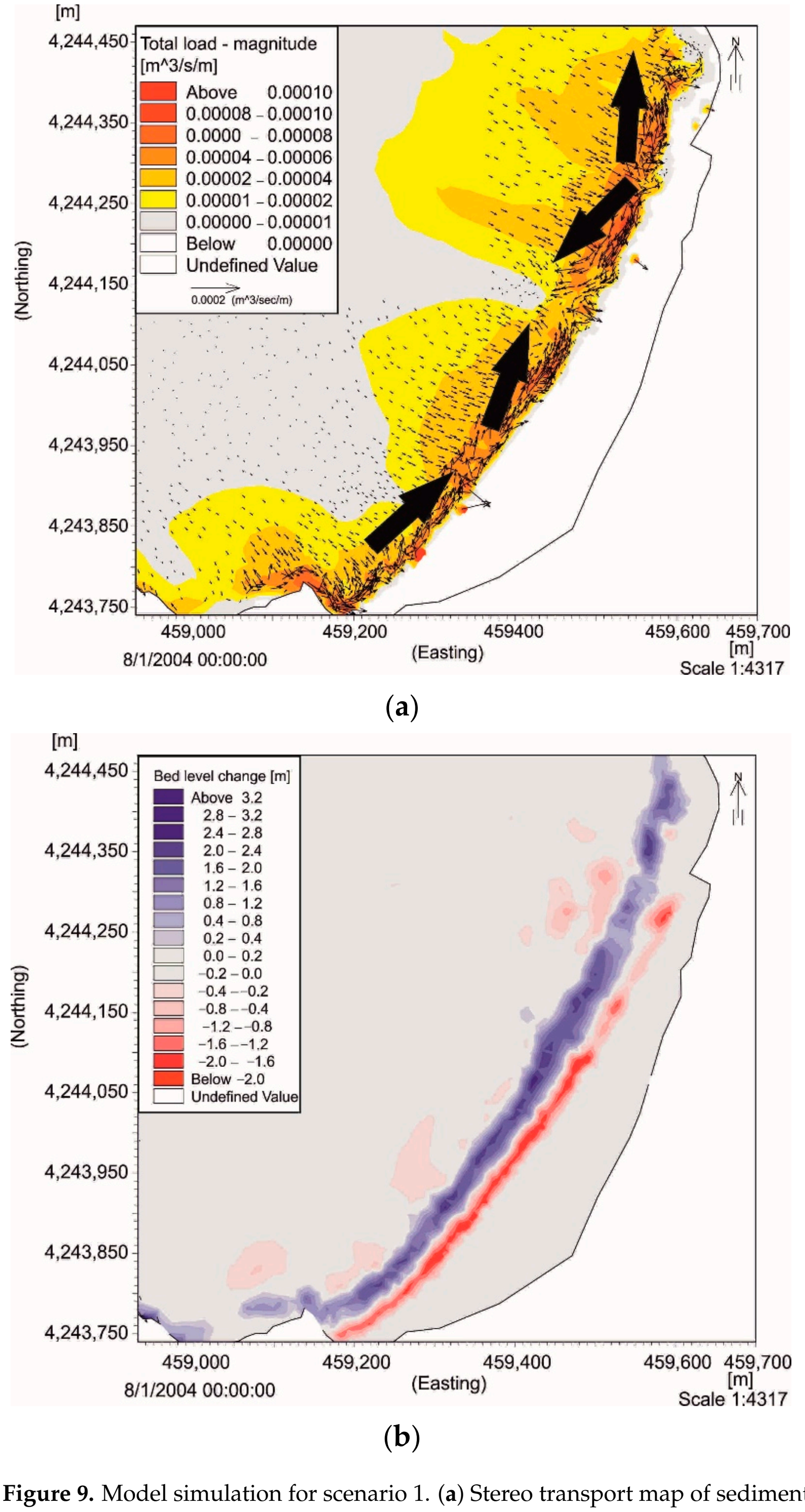

(**a**)

(**b**)

Figure 9. Model simulation for scenario 1. (**a**) Stereo transport map of sediments. (**b**) Map of seabed-level change. The arrows show the pattern of behavior of the (**a**) coastal sediment transportation.

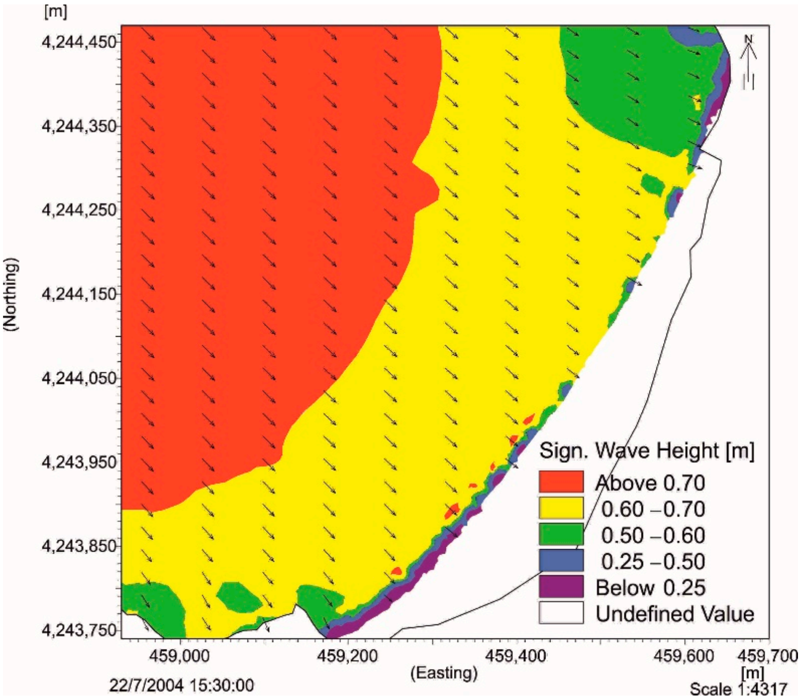

(**a**)

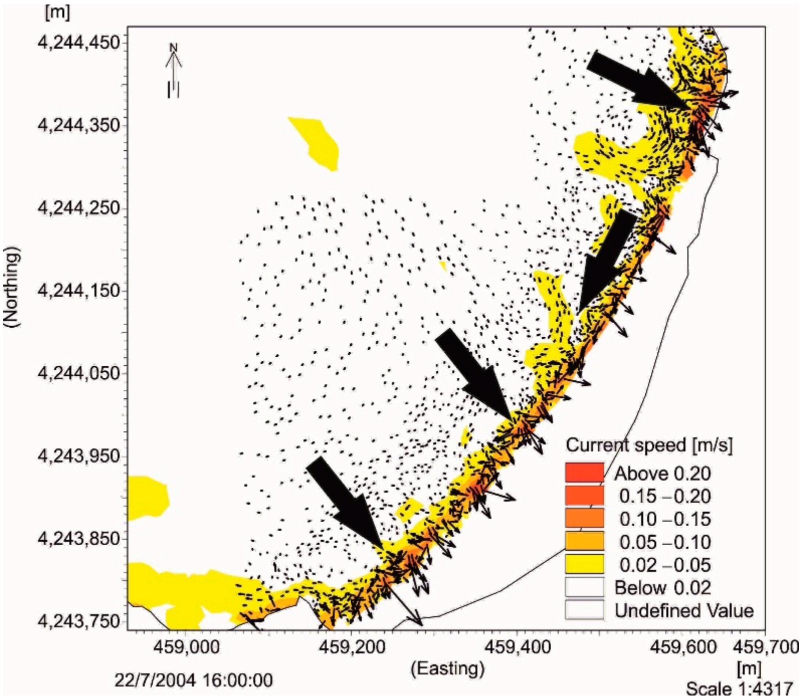

(**b**)

Figure 10. Model simulation for scenario 2. (**a**) Map of significant wave height distribution. (**b**) Map of coastal current velocity. The arrows show the pattern of behavior of the (**a**) Sign. wave and (**b**) current.

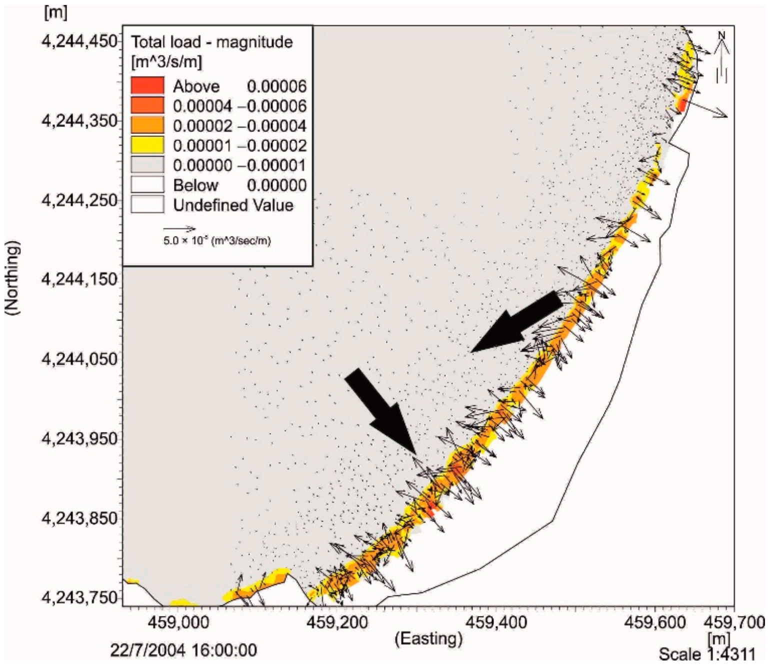

(**a**)

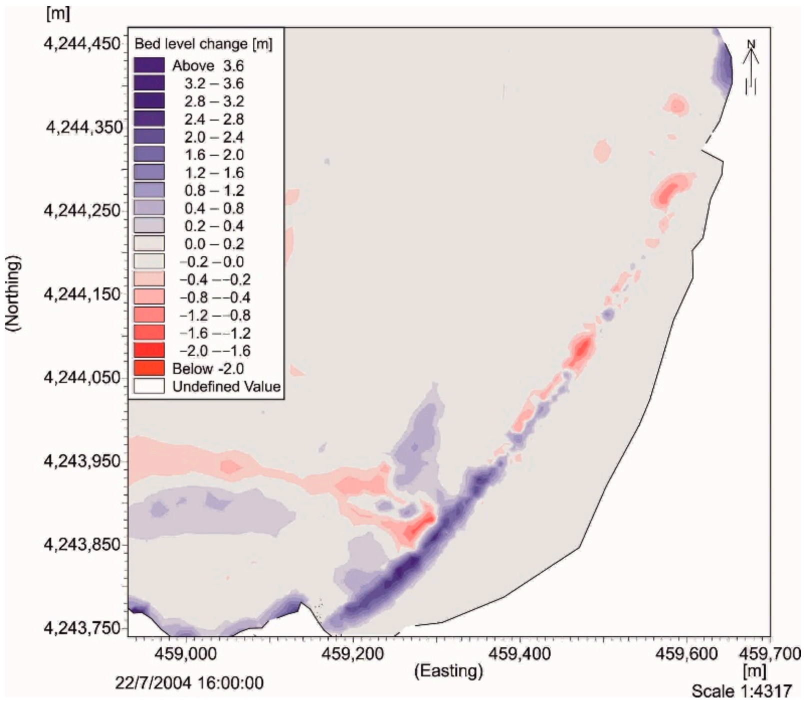

(**b**)

Figure 11. Model simulation for scenario 2. (**a**) Stereo transport map of sediments. (**b**) Map of seabed-level change. The arrows show the pattern of behavior of the (**a**) coastal sediment transportation.

In order to estimate the sediment volumes that were transported based on the two scenario simulations, the study area was separated into three sections. For each section, the sediment volumes transported on either side of each section for each scenario were quantified annually. The total sediment volume for Section 1 was estimated at 3047 m^3, directed to the southwest, and for Section 2, at 4744 m^3 in the same direction, causing erosion in the intermediate area. In Section 3, the transported sediment volumes were decreased (745 m^3), indicating a depositional environment in the southern part of the study area, between Sections 2 and 3 (Figure 12).

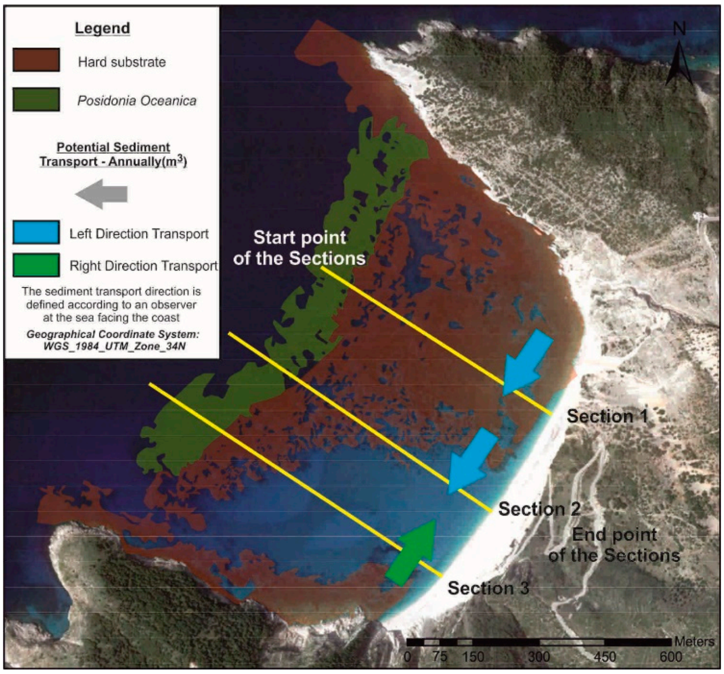

(a)

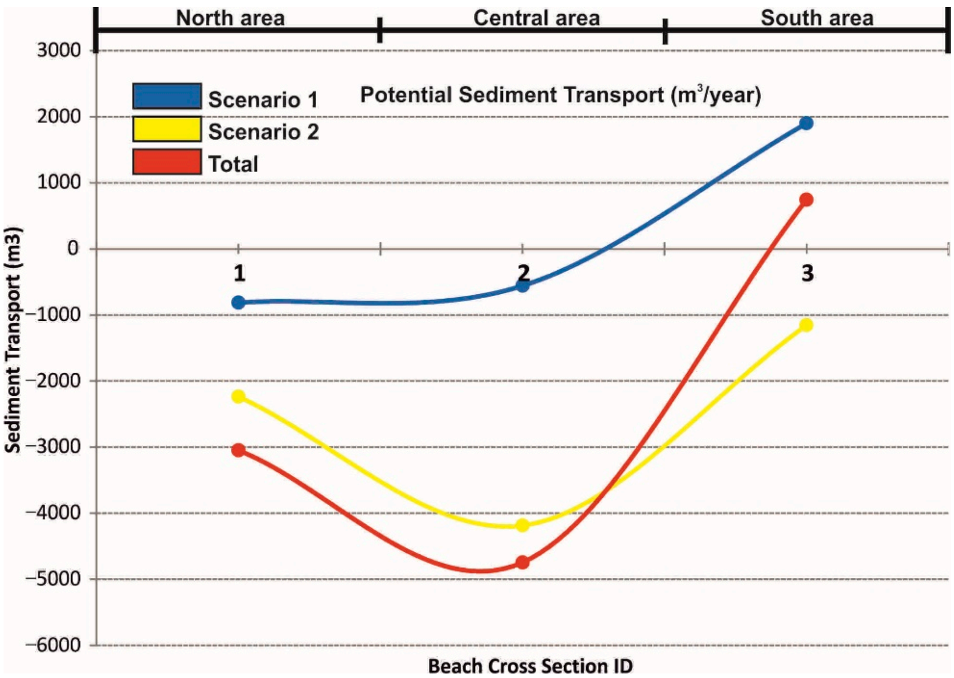

(b)

Figure 12. (**a**) A potential sediment direction that cross each section on an annual basis for scenarios 1 and 2, by dividing the study area in three sections. (**b**) An overall estimate (total) and volume of sediments that cross each section on an annual basis for scenarios 1 and 2, by dividing the study area in three sections.

Taking into account the data of wind and wave conditions for the study area [31–34] and the orientation of the coast, the most extreme event was on 24/11/2001 at 00:00; it was characterized by a mean wave height of 2.7 m, maximum wave height of 5.19 m, maximum wave period of 10.26 m, and mean wave direction of 304°, with a duration of 2.2 days. The highest values of wave height and wind speed were recorded on 24/11/2001 between 12:00 p.m. and 22:00 p.m. (wave height > 4 m, wind speed > 15 m/s) with a general wave direction of 307° and wind direction of 325° (Figure 13). For the specific time period, the average velocity of the coastal current was 0.22 m/s and the maximum value was 2.95 m/s, located at the southern part of the area with a NE direction. The actions of the coastal currents have the same impact at the coastal area as that which prevailed in scenario 1, with the formation of two longshore currents parallel to the coastline that are oriented from SW to NE and from NE to SW. The morphodynamics of the area favors the longshore current with a SW direction, and hence, it prevails over the one from NE direction; at the contact point a new current is created in the deeper parts of the bay with a SW direction. The average velocity of the longshore current with a SW direction is 0.4 m/s with a maximum of 2.5 m/s, whereas the average velocity for the current with a SW direction at the deepest parts of the bay is 0.45 m/s (maximum 0.83 m/s), up to the depth of 20 m (Figure 14a). Sediment transportation has a tendency to move from the surf zone to the deeper part perpendicular to the coast, especially in the area where the currents act. The largest volumes of coastal sediment transportation range from 1×10^{-5} to 3×10^{-3} m^3/sec/meter, with a prevailing orientation towards the deeper parts of the bay. Affected by the sediment transportation, seabed variation concerns the transport and deposition of sediments from the coast, and especially from the surf/wave zone to greater depths (10 m) at the central and south area, creating longshore bars at a distance of 100 m from the coastline, with a range of values between −2 m and 3.6 m (Figure 14b,c). It is worth noting that for the considered extreme event, small-scale hydrodynamic and sedimentary procedure occurred in the deepest parts of the bay and, specifically, in the SW sandy part, up to a depth of 33 m and at a distance of 750 m from the coastline.

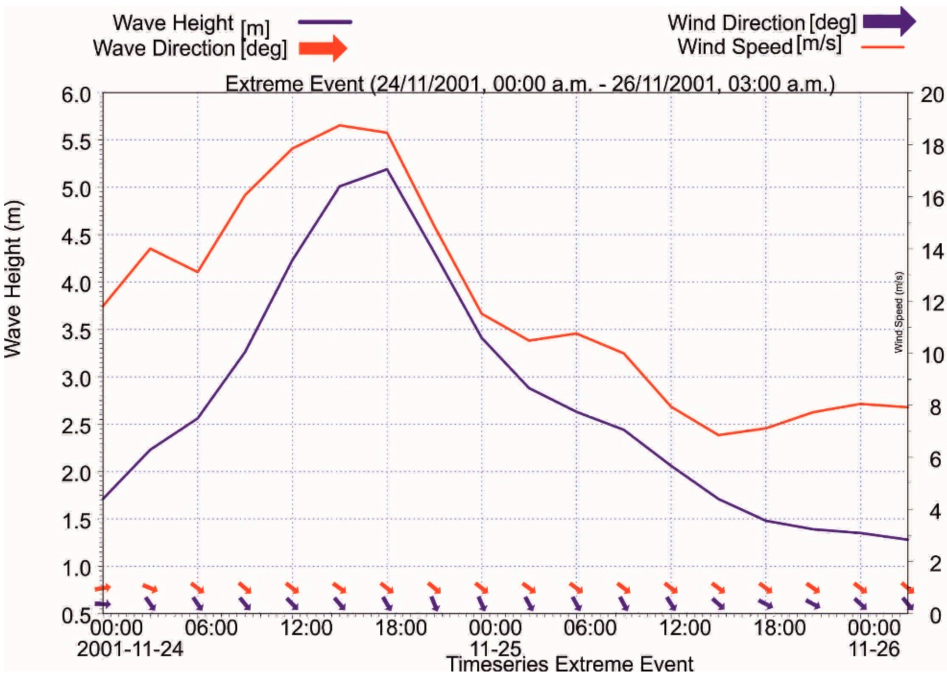

(**a**)

Figure 13. *Cont.*

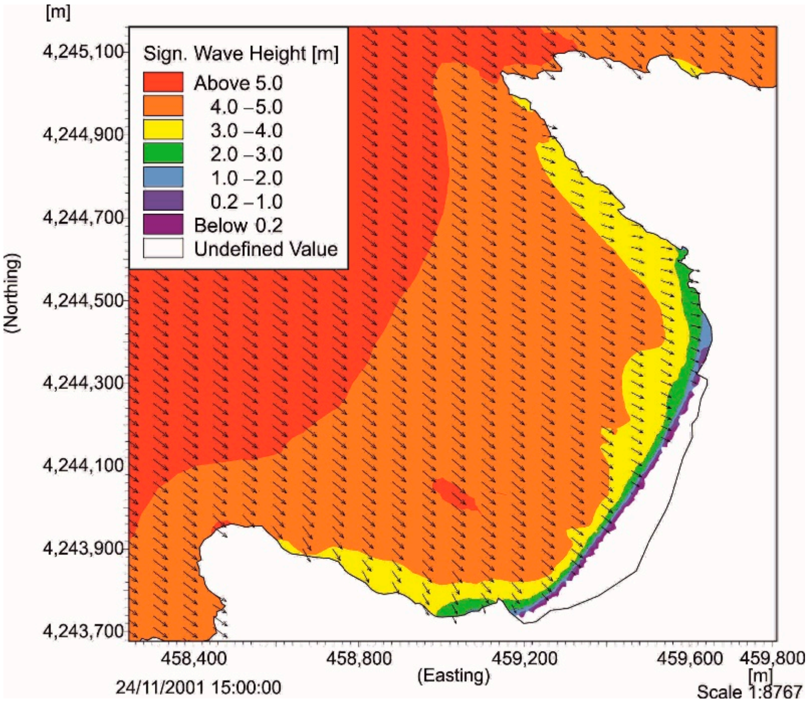

(**b**)

Figure 13. Model simulation for the maximum extreme event. (**a**) Diagram of the wind and wave conditions of the time period in which the extreme event occurred. (**b**) Map of significant wave height distribution. The arrows show the pattern of behavior of the (**b**) Sign. wave.

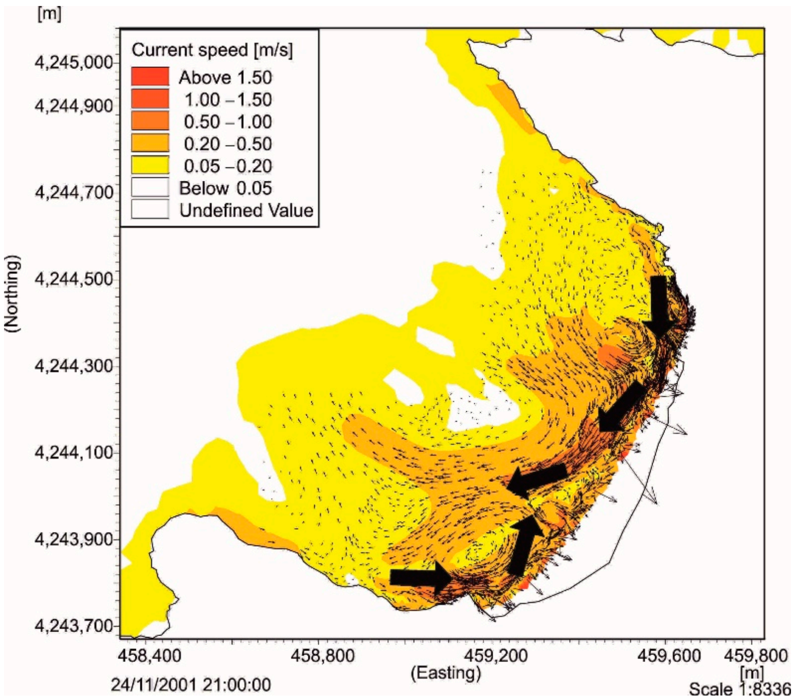

(**a**)

Figure 14. *Cont*.

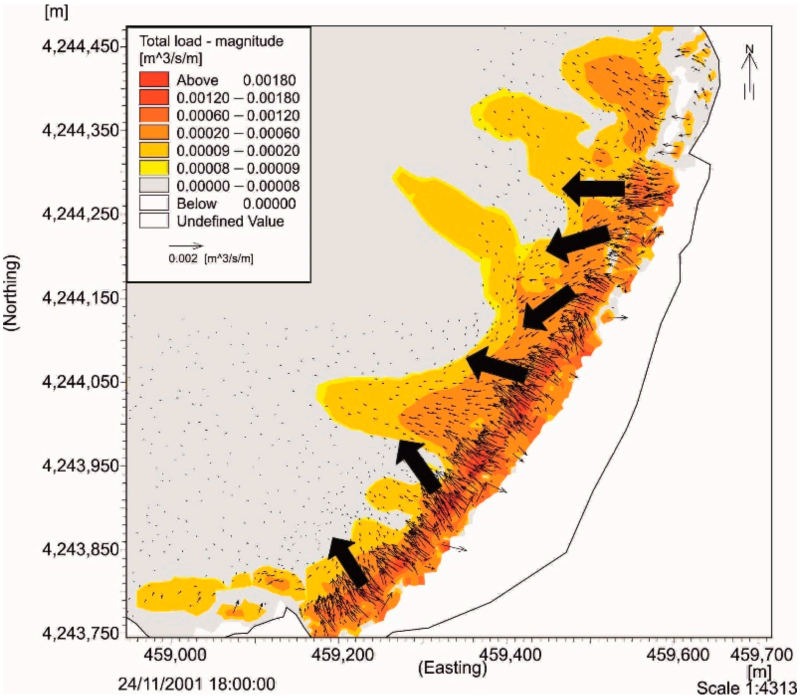

(**b**)

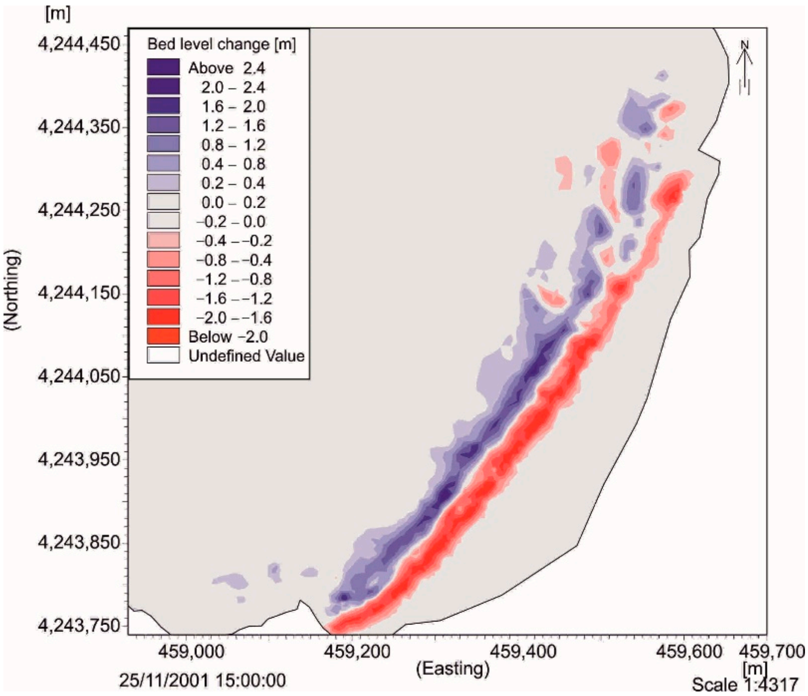

(**c**)

Figure 14. Model simulation for the maximum extreme event. (**a**) Map of coastal current velocity. (**b**) Stereo transport map of sediments. (**c**) Map of seabed-level change. The arrows show the pattern of behavior of the (**a**) current and the (**b**) coastal sediment transportation.

5. Discussion

The wider area of Myrtos is a part of a constantly evolving process, controlled by both the intense geodynamic neotectonic processes (onshore/offshore) and hydrometeorological phenomena. These processes form a geotechnically unstable area, affecting its morphology, such as bathymetry and topography, whereas landslides that are caused mainly at the northern part of the cliff constitute the main sediment supply to Myrtos Beach [28,29,47,50].

The topographic, sedimentological, and morphodynamic seasonal analysis of the coastal area during 10/2018 and 03/2019 and the morphological profile sections revealed the seasonal fluctuations between those two periods, with erosion patterns in the winter months by the more energetic waves, and sedimentation during the summer months [26,57–60]. In all sections and mainly in Beach Profile 3 (Figure 4), the sediment deposition during the summer period was recorded over the winter deposits, revealing a progression in sediment loss or gain along successive beach profiles. Additionally, beach berms were noticed along the cross sections at the beach face and were characterized by steep slopes and coarse sediments that followed the weather profile, becoming also a frequent practice to buffer coastal erosion. The gravelly sand to coarse gravel sediment composition of the beach is characterized by heterogeneous properties, and the sediments are located in high-energy environments [61], with the coarser sediments located landward and well sorted, and at the dynamic swash zone different sediment sizes are found which are poorly sorted [4,62,63].

The summer beach berms present a smoother topography, formed as a result of low energy swelling waves, whereas the winter beach berms are formed in large numbers with a limited extent due to storm events. The fluctuations between the topography and sedimentology indicates the importance of morphodynamic stages and, consequently, energy levels [64,65]. The different behavior of the beach profiles, mainly at the surf zone, is related to the cross-shore and longshore transportation perpendicular or at an angle to the shore, caused by the combined action of wind and waves and shore currents; the coarser material suggests its origin from landslides, which, in combination with the prevailing hydrodynamic conditions, play an important role in the sedimentation of the area [2,66]. The evaluation of the shoreline displacement at a seasonal scale (short-to-medium-term analysis) reveals that beach rotation (erosion at one end of the coast with deposition at the other end) is common and can result from seasonal fluctuations that affect waves [66–68]. The influence of landslides in the area can be identified through the evolution of the shoreline, as from 2003 to 2013 there was a tendency of retreat in most of the beach (Figure 15a); then, in 2014 two earthquakes occurred in the area, causing landslides and rock falls on Myrtos Beach [28,29,47,48,50]. This resulted in the supply of the beach with large volumes of material, causing shoreline progradation of about 15 m during the period 2013–2019 (Figure 15b). The advance rate varied between 1.4 m/year at both edges of the coast and 2.5 m/year in the central part of the beach. These rates are indicative for the period 2013–2019, as after each landslide the values change.

The numerical model indicates that for both annual representative scenarios and the extreme event, the prevailing morphodynamic and hydrodynamic conditions are identical. As the wind-induced waves are decisive for the hydrodynamic circulation of the pocket beach, wind direction and beach orientation, are two crucial parameters for the produced longshore currents.. The only difference is in the value range for each category (e.g., coastal current velocity, total load of sediment transported, seabed-level change) and the duration of the simulation, as depending on wave energy conditions, the hydrodynamic circulation can rapidly change. Scenario 2, although with low values, prevailed in the morphodynamic formation of the bay due to the long-term simulation (203 days), according to the annually maximum wind-induced wave energy flux from that direction (315°) [41,51–55] (Table 4). The hydrodynamic conditions formed by the specific scenarios create a typical circular surface current pattern developed in pocket beaches by two wave-induced longshore currents parallel to the coast in opposite directions (SW to NE for the southern part of the beach and NE to SW for the northern part) [12], making them the major contributor to sediment transport along the shoreface. Due to the morphology of the seabed and the dominance of the hard substrate in the northern area, the currents coming from the north prevail over the others, with the sediment transportation taking place mainly in the central part, but also in the deeper parts of the southern bay. This confirms that the geomorphological substrate controls the location and intensity of coastal currents. An anti-clockwise circulation pattern was also observed in the southern part of the area, enhancing the assumption of sedimentation at that certain area. In fact, the sediment transportation at the bay is determined by the combination of the current and wave direction. The currents that dominated at the coastal area are produced according to the wave-induced current. Therefore, the morphological changes of the beach (e.g., longshore bar, beach berm, erosion/deposition area) and the direction of those features demonstrate that the prevailing significant waves with high-energy flux, depending on their approaching direction, play a major role in sediment transportation along the coast [39,69]

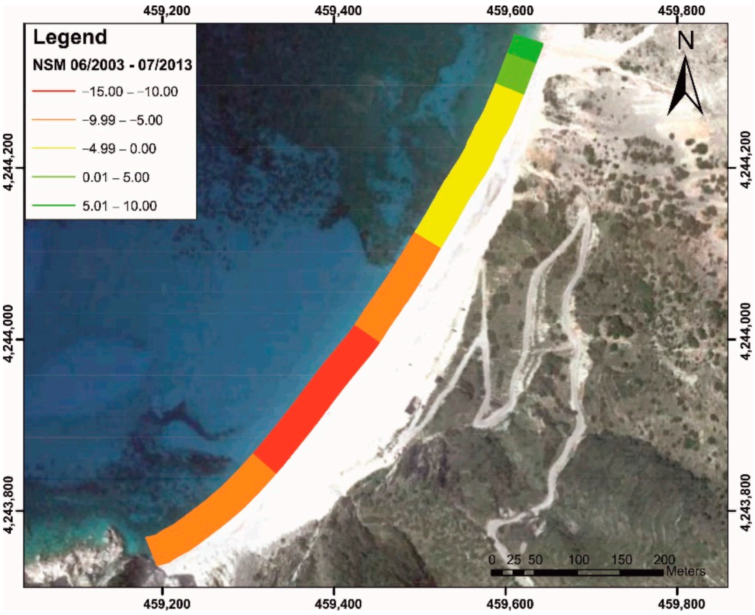

(**a**)

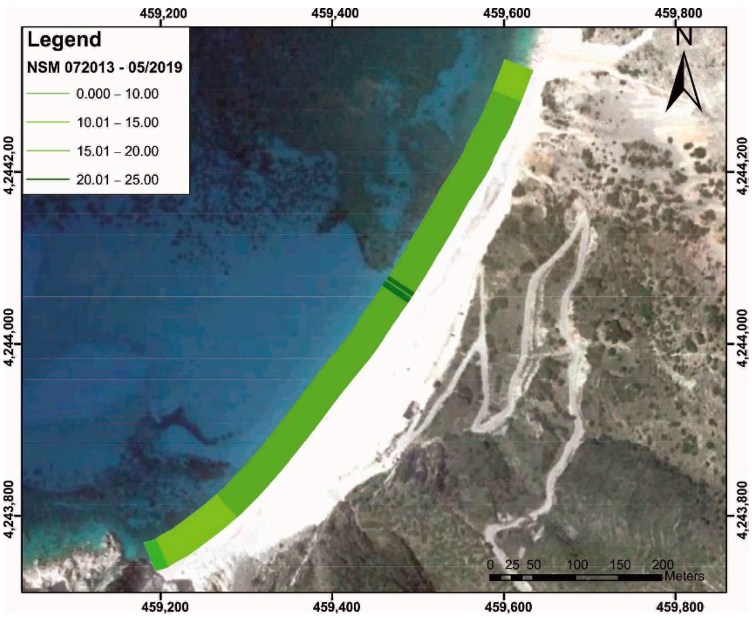

(**b**)

Figure 15. Net shoreline movement at Myrtos Beach. The figures display the size of coastline fluctuation for the periods (**a**) 2003–2013 and (**b**) 2013–2019. In 2014 two earthquakes occurred in the area, causing landslides and rock falls on Myrtos Beach [28,29,47,48,50], causing shoreline progradation.

Table 4. Potential sediment transport (m^3/year). The sediment transport direction is defined according to an observer on the sea, facing the coast. The negative values indicate a transport to the right and positive values indicate a transport to the left.

	Scenario 1	Scenario 2	Extreme Event
Section 1	−811.848	−2235.61	−638.776
Section 2	−558.566	−4184.97	−872.509
Section 3	1900.41	−1155.65	5680.17

According to Table 4 and and Figure 16a,b the current patterns from the simulations, the largest sediment volume is transported from the northern (Section 1) to the central and southern part of the coast (Sections 2 and 3); a large percentage of sediment is deposited near the coast down to a 10 m depth between Sections 2 and 3, whereas in extreme events it can reach deeper parts of the bay, down to a 34 m depth. In addition, the formation of longshore bars indicates sediment removal and transportation from the coast, causing sea bottom fluctuations mainly up to the break zone. In these areas, the breaking waves increase the accumulation of sandy sediments due to increased local bed shear stress and form longshore bars [70].

These observations suggest that beach morphodynamic, hydrodynamic, topographic, and sedimentological functions of a pocket beach (limited by headlands) are a part of the geological/geodynamic condition of the area (e.g., coast orientation, substrate mapping, coastal plain morphology, sediment source) and hydrodynamic factors (e.g., wind/wave condition, currents, sediment transportation, longshore bar). As the headlands act as a physical barrier to any renourishment from neighboring coasts, Myrtos Bay shows a certain ability to retain sediments, enhancing their movement between this area despite the high intensity wind-induced waves and currents, creating a local morphodynamic/hydrodynamic environment [1,3,10,12]. Essentially, the Myrtos pocket beach is considered to behave with its own limited sediment supply, recycling sediments between the nearshore, foreshore, and backshore. This work showed that the sediment fluxes carried mainly by longshore and rip currents until water depths of 10 m for the annual scenario and 33 m for the extreme wave event were a function of the direction and energy of wave-induced flux, of the substrate type, of the coast morphology, and of the sediment characteristics. The sedimentary material coming from the landward part is also notable; the sediment supply derives almost entirely from the landslide material from the neighboring cliffs and in relation to the prevailing hydrodynamic/topographic factors; they are deposited in the central and southern area of the bay. Landslides are characterized as episodic events that occur relatively often because the force of the earthquake, heavy rainfall (flash floods), human activity, and wave erosion disturb the natural stability of a slope (gravity moves), offering significant volumes of sediment to the Myrtos pocket beach during these events [18].

It is generally accepted that climate change has resulted in a further rise in global sea-levels [71–73] and, consequently, many coastal areas' susceptibility to floods has increased [74]. The coastal zone is among the most densely populated and fastest-growing areas on Earth, and these areas need to be viewed as interactive systems, including both human and physical components [75,76]. The sustainability of coastal environments depends on understanding these interactions. The pressures that intense human use brings are exacerbated by climate change, particularly the observed and anticipated sea-level rise, which increases coastal erosion and inundation, resulting in habitat loss and causing what has been called "coastal squeeze" as well as impacting local populations and tourism [77]. The overall rise in the sea-level is expected to directly affect coastal human activities and infrastructure, as well as cultural and geological heritage, agriculture, and biodiversity [78–80].

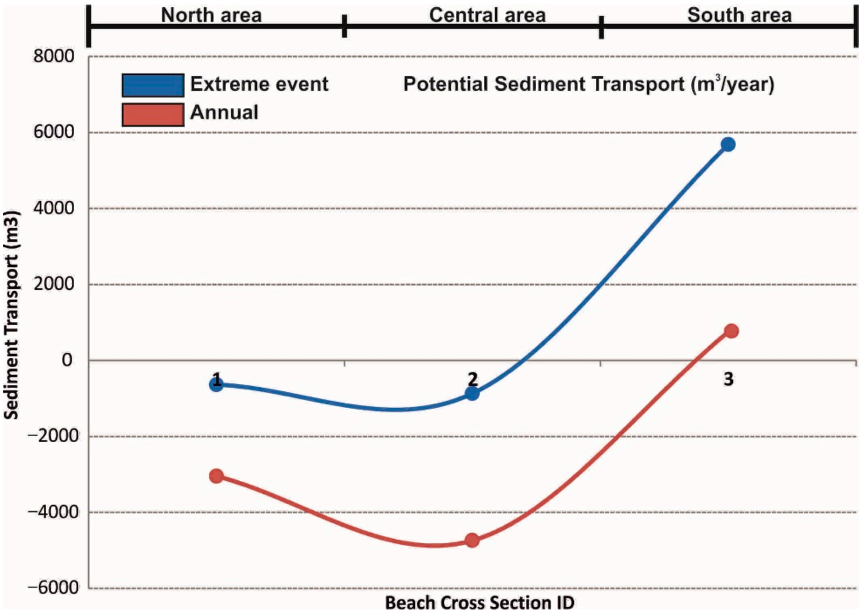

(**a**)

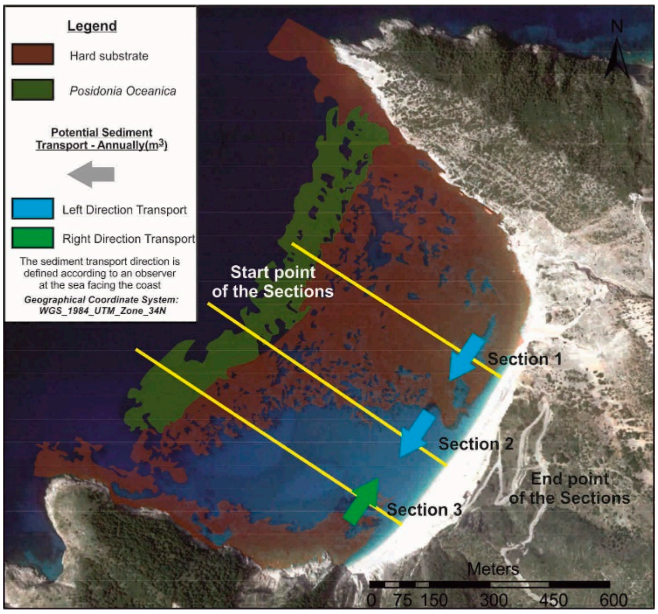

(**b**)

Figure 16. (**a**) An overall estimate (total) and volume of sediments that cross each section on an annual basis and in an extreme event, by dividing the study area in three sections. (**b**) A potential sediment direction that cross each section on an annual basis by dividing the study area in three sections.

In this sense, our findings between hydrodynamic and sediment circulation, geomorphology, and the geological context (embayed setting, landslides, rocky shoreface) may be crucial for better management by the local authorities, as any inappropriate method will degrade the quality of the environment and directly affect the environmental and economic sustainability of the wider area. Risk management policies focus on structural defense investments, such as reinforcing slope material, installation of structures such as piles and retaining walls, diversion of debris pathways, and rerouting of surface and underwater drainage. Such methods aim to protect the affected area from landslides, but they also significantly reduce the sedimentary material offered by landslides.

Any method of a “hard/soft technique” that is going to be used must be environmentally acceptable in order to maintain a dynamic balance of the natural system of the coastal area [81–83]. The investment in structural defense should be focused on soil management in relation to landslide prevention, combining this with the economic and tourist development of the wider area with regard to security and sustainability.

6. Conclusions

The coastal morphodynamics of the Myrtos pocket beach was investigated through in situ measurements and statistical and numerical models, with the aim to evaluate its short and medium-to-long-term dynamics. Our study revealed a dynamic condition with a high-energy environment and results showing an environment under deposition. Specifically, in a short-term analysis, the beach profiles allowed the characterization of a high-energy environment with coarse sediments and with seasonal fluctuations in the topography and the granulometry, responding to the different weather conditions prevailing in the area for each period. Through the satellite images, shoreline progradation was noted with an advance rate close to 2 m/year for the period 2013–2019 and after two landslides that occurred from the 2014 earthquakes. The extensive field work, laboratory analysis, and hydrographical and sediment transport model simulations presented in this work confirmed sediment transportation and deposition that is mainly at the coastal region from the northern to the central and southern part of the bay, developing the expected circular pattern that characterizes a typical pocket beach. In an extreme event, this transportation and sedimentation can take place in deeper areas. However, all the sediment dynamics take place between the two headlands that isolate the bay, whereas the sediment sources are exclusively material deriving from landslides.

Our findings may be used for practical approaches to achieve a better environmental and economic management of the coastal area seeking dynamic equilibrium by creating a static bay pocket beach that can remain stable without requiring external contribution. Any activity that is to be implemented, such as a defense structure to stabilize landslides, should not have any negative consequences for the development of the beach, as any change to beach sediment budget, sediment characteristics, morphology, and hydrodynamics is critical for long-term changes and the preservation of pocket beaches for future human use considering climate change.

Supplementary Materials: The following supporting information can be downloaded at: https://www.mdpi.com/article/10.3390/jmse10081015/s1, Figure S1: Lithological and geomorphological map of the study area. Geology based on geological map of Greece (1:50,000), Cephalonia Island (northern part), Institute of Geology and Mineral Exploration; Figure S2: (a) Wind and (b) wave rose diagram for the study area from1995 to 2004; Figure S3. Field survey that was carried out during 10/2018 and 05/2019; Figure S4: The direction of Myrtos Bay ranges between 265° and 343°, whereas the orientation of the coastline is 304°; the two representative scenarios that contribute to the sediment transport from one side to the other and in the opposite direction are scenario 1: 264–304° and scenario 2: 305–343°.

Author Contributions: Conceptualization, A.P., V.K. and N.E.; methodology, V.K., A.P.; software, A.P.; validation, V.K., A.P.; formal analysis, V.K., N.E., A.K. and A.P.; investigation, A.P. and K.G.; data curation, A.P. and K.G.; writing—original draft preparation, A.P.; writing—review and editing, V.K., A.K., N.E. and A.P.; visualization, A.K. and A.P.; supervision, V.K., A.K., N.E. and A.P. All authors have read and agreed to the published version of the manuscript.

Funding: Alexandros Petropoulos have been awarded with a scholarship for their PhD research from the "1st Call for PhD Scholarships by HFRI"–"Grant Codes 1812", from the General Secretariat for Research and Technology (G.S.R.T.) and the Hellenic Foundation for Research and Innovation (H.F.R.I.).

Acknowledgments: Special thanks to the Hellenic Centre for Marine Research (HCMR) for the supply of scientific equipment.

Conflicts of Interest: The authors declare no conflict of interest.

References

1. Short, A.D.; Masselink, G. Embayed and structurally controlled beaches. In *Handbook of Beach and Shoreface Morphodynamics*; Short, A.D., Ed.; John Wiley and Sons Ltd.: Chichester, UK, 1999; pp. 230–249.
2. Bowman, D.; Guillén, J.; López, L.; Pellegrino, V. Planview Geometry and morphological characteristics of pocket beaches on the Catalan coast (Spain). *Geomorphology* **2009**, *108*, 191–199. [CrossRef]
3. Dehouck, A.; Dupuis, H.; Sénéchal, N. Pocket beach hydrodynamics: The example of four macrotidal beaches, Brittany, France. *Mar. Geol.* **2009**, *266*, 1–17. [CrossRef]
4. Vousdoukas, M.I.; Velegrakis, A.F.; Dimou, K.; Zervakis, V.; Conley, D.C. Wave run-up observations in microtidal, sediment-starved pocket beaches of the Eastern Mediterranean. *J. Mar. Syst.* **2009**, *78*, S37–S47. [CrossRef]
5. Storlazzi, C.D.; Field, M.E. Sediment distribution and transport along a rocky, embayed coast: Monterey Peninsula and Carmel Bay, California. *Mar. Geol.* **2000**, *170*, 289–316. [CrossRef]
6. Short, A.D. *Handbook of Beach and Shoreface Morphodynamics*; John Wiley & Sons: New York, NY, USA, 1999; ISBN 0-471-96570-7.
7. Klein, A.H.F.; Ferreira, Ó.; Dias, J.M.A.; Tessler, M.G.; Silveira, L.F.; Benedet, L.; de Menezes, J.T.; de Abreu, J.G.N. Morphodynamics of structurally controlled headland-bay beaches in southeastern Brazil: A review. *Coast. Eng.* **2010**, *57*, 98–111. [CrossRef]
8. Hsu, J.R.C.; Yu, M.J.; Lee, F.C.; Benedet, L. Static bay beach concept for scientists and engineers: A review. *Coast. Eng.* **2010**, *57*, 76–91. [CrossRef]
9. Daly, C.J.; Bryan, K.R.; Gonzalez, M.R.; Klein, A.H.F.; Winter, C. Effect of selection and sequencing of representative wave conditions on process-based predictions of equilibrium embayed beach morphology. *Ocean Dyn.* **2014**, *64*, 863–877. [CrossRef]
10. Oliveira, S.; Moura, D.; Horta, J.; Nascimento, A.; Gomes, A.; Veiga-Pires, C. The morphosedimentary behaviour of a headland–beach system: Quantifying sediment transport using fluorescent tracers. *Mar. Geol.* **2017**, *388*, 62–73. [CrossRef]
11. Short, A.D.; Trembanis, A.C.; Turner, I.L. Beach oscillation, rotation and the Southern Oscillation, Narrabeen Beach, Australia. In Proceedings of the Coastal Engineering 2000—27th International Conference on Coastal Engineering, Sydney, Australia, 16–21 July 2000; pp. 2439–2452. [CrossRef]
12. Castelle, B.; Coco, G. The morphodynamics of rip channels on embayed beaches. *Cont. Shelf Res.* **2012**, *43*, 10–23. [CrossRef]
13. Goda, Y. Reanalysis of regular and random breaking wave statistics. *Coast. Eng.* **2010**, *52*, 71–106. [CrossRef]
14. Balouin, Y.; Belon, R. Evolution of Corsican pocket beaches. In Proceedings of the 13th International Coastal Symposium, Durban, South Africa, 13 April 2014; Green, A.N., Cooper, J.A.G., Eds.; pp. 96–101.
15. Brunel, C.; Sabatier, F. Potential influence of sea-level rise in controlling shoreline position on the French Mediterranean Coast. *Geomorphology* **2009**, *107*, 47–57. [CrossRef]
16. Horta, J.; Oliveira, S.; Moura, D.; Ferreira, Ó. Nearshore hydrodynamics at pocket beaches with contrasting wave exposure in southern Portugal. *Estuar. Coast. Shelf Sci.* **2018**, *204*, 40–55. [CrossRef]
17. Norcross, Z.M.; Fletcher, C.H.; Merrifield, M. Annual and interannual changes on a reef-fringed pocket beach: Kailua Bay, Hawaii. *Mar. Geol.* **2002**, *190*, 553–580. [CrossRef]
18. Sallenger, A.H.; Krabill, W.; Brock, J.; Swift, R.; Manizade, S.; Stockdon, H. Sea-cliff erosion as a function of beach changes and extreme wave runup during the 1997-1998 El Niño. *Mar. Geol.* **2002**, *187*, 279–297. [CrossRef]
19. Anthony, E.J.; Gardel, A.; Dolique, F.; Guiral, D. Short-term changes in the plan shape of a sandy beach in response to sheltering by a nearshore mud bank, Cayenne, French Guiana. *Earth Surf. Process. Landf.* **2002**, *27*, 857–866. [CrossRef]
20. Dalrymple, R.A.; MacMahan, J.H.; Reniers, A.J.H.M.; Nelko, V. Rip currents. *Annu. Rev. Fluid Mech.* **2011**, *43*, 551–581. [CrossRef]
21. Van Dongeren, A.; Lowe, R.; Pomeroy, A.; Trang, D.M.; Roelvink, D.; Symonds, G.; Ranasinghe, R. Numerical modeling of low-frequency wave dynamics over a fringing coral reef. *Coast. Eng.* **2013**, *73*, 178–190. [CrossRef]
22. Billi, P.; Fazzini, M. Global change and river flow in Italy. *GPC* **2017**, *155*, 234–246. [CrossRef]
23. Hsu, J.R.-C.; Benedet, L.; Klein, A.H.F.; Raabe, A.L.A.; Tsai, C.P.; Hsu, T.W. Appreciation of static bay beach concept for coastal management and protection. *J. Coast. Res.* **2008**, *24*, 198–215. [CrossRef]
24. Dean, R.G. Equilibrium beach profiles: Characteristics and applications. *J. Coast. Res.* **1991**, *7*, 53–84.
25. Karunarathna, H.; Horrillo-Caraballo, J.M.; Reeve, D.E. Prediction of cross-shore beach profile evolution using a diffusion type model. *Cont. Shelf Res.* **2012**, *48*, 157–166. [CrossRef]
26. Anfuso, G.; Pranzini, E.; Vitale, G. An integrated approach to coastal erosion problems in northern Tuscany (Italy): Littoral morphological evolution and cell distribution. *Geomorphology* **2011**, *129*, 204–214. [CrossRef]
27. Papanikolaou, D. *Geology of Greece*, 1st ed.; Pataki: Athens, Greece, 2015; ISBN 978-960-16-6343-2.
28. Lekkas, E.; Mavroulis, S. Fault zones ruptured during the early 2014 Cephalonia Island (Ionian Sea, Western Greece) earthquakes (January 26 and February 3, Mw 6.0) based on the associated co-seismic surface ruptures. *J. Seismol.* **2016**, *20*, 63–78. [CrossRef]
29. Lekkas, E.L.; Mavroulis, S.D. Earthquake environmental effects and ESI 2007 seismic intensities of the early 2014 Cephalonia (Ionian Sea, western Greece) earthquakes (January 26 and February 3, Mw 6.0). *Nat. Hazards* **2015**, *78*, 1517–1544. [CrossRef]
30. Saroglou, H. Rockfall susceptibility in Greece and study of coseismic events. In Proceedings of the 15th Symposium on Engineering Geology & Geotechnics, Belgrade, Serbia, 22–23 September 2016; pp. 19–35.
31. Soukisian, T.; Hatzinaki, M.; Korres, G.; Papadopoulos, A.; Kallos, G.; Anadranistakis, E. *Wind and Wave Atlas of the Hellenic Seas*, 1st ed.; Hellenic Centre for Marine Research: Athens, Greece, 2007; ISBN 987 960 86651 9-4.

32. Haiden, T.; Janousek, M.; Bauer, P.; Bidlot, J.-R.; Dahoui, M.; Ferranti, L.; Prates, F.; Richardson, D.; Vitart, F. *Evaluation of ECMWF Forecasts, including 2014-2015 Upgrades*; ECMWF: Reading, UK, 2015; 7p.
33. *Deltares Product User Guide for Sea Level and Ocean Wave Products-Time Series and Indicators C3S_422_Lot2_Deltares-European Services*; ECMWF: Reading, UK, 2019.
34. Sifnioti, D.; Soukissian, T.; Poulos, S.; Nastos, P.; Hatzaki, M. Evaluation of in-situ wind speed and wave height measurements against reanalysis data for the Greek Seas. *Mediterr. Mar. Sci.* **2017**, *18*, 486–503. [CrossRef]
35. Folk, R.L.; Ward, W.C. Brazos River bar [Texas]; a study in the significance of grain size parameters. *J. Sediment. Res.* **1957**, *27*, 3–26. [CrossRef]
36. Blott, S.J.; Pye, K. GRADISTAT: A grain size distribution and statistics package for the analysis of unconsolidated sediments. *Earth Surf. Processes Landf.* **2001**, *26*, 1237–1248. [CrossRef]
37. Thieler, E.R.; Himmelstoss, E.A.; Zichichi, J.L.; Ergul, A. *The Digital Shoreline Analysis System (DSAS) Version 4.0—An ArcGIS Extension for Calculating Shoreline Change*; U.S. Geological Survey: Reston, VA, USA, 2009.
38. Anfuso, G.; Bowman, D.; Danese, C.; Pranzini, E. Transect based analysis versus area based analysis to quantify shoreline displacement: Spatial resolution issues. *Environ. Monit. Assess.* **2016**, *188*, 568. [CrossRef]
39. Sedrati, M.; Anthony, E.J. A brief overview of plan-shape disequilibrium in embayed beaches: Tangier bay (Morocco). *J. Mediterr. Geogr.* **2007**, *108*, 125–130. [CrossRef]
40. Balas, L.; Inan, A. A Numerical Model of Wave Propagation on Mild Slopes. *J. Coast. Res.* **2002**, *36*, 16–21. [CrossRef]
41. Petropoulos, A.; Evelpidou, N.; Kapsimalis, V.; Anagnostou, C.; Karkani, A. Sediment transport patterns and beach morphodynamics in the semi-enclosed bay of Platis Gialos, Sifnos Island, Aegean Sea. *Z. Geomorphol.* 2021; *in press*. [CrossRef]
42. MIKE powered by DHI. *MIKE 21 Wave Modelling, MIKE 21 Spectral Waves FM*; DHI: Horsholm, Denmark, 2017.
43. Bulhoes, E.; Fernandez, G.B. Analysis of shallow water wave propagation and coastal response in embayed beaches. Case study in Cape Buzios, Rio de Janeiro, Brazil. *J. Coast. Res.* **2011**, *SI64*, 2022–2026.
44. Jose, F.; Kobashi, D.; Stone, G.W. Spectral wave transformation over an elongated sand shoal off south-central Louisiana, USA. *J. Coast. Res.* **2007**, *SI50*, 757–761.
45. Hallermeier, R.J. A profile zonation for seasonal sand beaches from wave climate. *Coast. Eng.* **1980**, *4*, 253–277. [CrossRef]
46. Zou, Q.; Xie, D. Tide-surge and wave interaction in the Gulf of Maine during an extratropical storm. *Ocean. Dyn.* **2016**, *66*, 1715–1732. [CrossRef]
47. Valkaniotis, S.; Ganas, A.; Papathanassiou, G.; Papanikolaou, M. Field observations of geological effects triggered by the January–February 2014 Cephalonia (Ionian Sea, Greece) earthquakes. *Tectonophysics* **2014**, *630*, 150–157. [CrossRef]
48. Papathanassiou, G.; Valkaniotis, S.; Ganas, A. Evaluation of the macroseismic intensities triggered by the January/February 2014 Cephalonia, (Greece) earthquakes based on ESI-07 scale and their comparison to 1867 historical event. *Quat. Int.* **2017**, *451*, 234–247. [CrossRef]
49. Saroglou, H.; Asteriou, P.; Tsiambaos, G.; Zekkos, D.; Clark, M.K.; Manousakis, J. Investigation of Two Co-Seismic Rockfalls During the 2015 Lefkada and 2014 Cephalonia Earthquakes in Greece. In Proceedings of the 3rd North American Symposium on Landslides, Roanoke, VA, USA, 4–8 June 2017; pp. 521–528.
50. Theodoulidis, N.; Karakostas, C.; Lekidis, V.; Makra, K.; Margaris, B.; Morfidis, K.; Papaioannou, C.; Rovithis, E.; Salonikios, T.; Savvaidis, A. The Cephalonia, Greece, January 26 (M6.1) and February 3, 2014 (M6.0) earthquakes: Near-fault ground motion and effects on soil and structures. *Bull. Earthq. Eng.* **2016**, *14*, 1–38. [CrossRef]
51. Coastal Engineering Research Center (CERC). *Shore Protection Manual*; US Army Corps of Engineers, Ed.; Scientific Research Publishing: Washington, DC, USA, 1984; Volume I-I.
52. Borah, D.K.; Balloffet, A. Beach Evolution Caused by Littoral Drift Barrier. *J. Waterw. Port Coast. Ocean. Eng.* **1985**, *111*, 645–660. [CrossRef]
53. *IEC TS 62600-101*; Marine Energy—Wave, Tidal and Other Water Current Converters—Part 101: Wave Energy Resource Assessment and Characterization. 1st ed. International Electrotechnical Commission (IEC): Geneva, Switzerland, 2015; ISBN 978-2-8322-2724-4.
54. Tucker, M.J.; Malcolm, J.; Pitt, E.G. *Waves in Ocean Engineering*, 1st ed.; Tucker, M.J., Malcolm, J., Pitt, E.G., Eds.; Elsevier Science & Technology: Oxford, UK, 2001; ISBN 9780080435664.
55. Kapsimalis, V.; Gad, F.K. Research, Study of the Coastal Zone and the Marine Area of the Gulf of Chania. Coastal Engineering Investigation of the Coastal Zones of Kolimbari-Tavronitis & Platania-Kato Stalou. In *Study of Erosion and Protection of the Coasts of the Gulf of Chania*; H.C.M.R.: Athens, Greek, 2016.
56. Gad, F.K.; Chatzinaki, M.; Vandarakis, D.; Kyriakidou, C.; Kapsimalis, V. Assessment of wave storm-induced flood vulnerability in rhodes island, greece. *Water* **2020**, *12*, 2978. [CrossRef]
57. Cooper, N.J.; Barber, P.C.; Bray, M.J.; Carter, D.J. Shoreline management plans: A national review and engineering perspective. In *Proceedings of the Institution of Civil Engineers—Water and Maritime Engineering*; Thomas Telford Ltd.: London, UK, 2002; Volume 154, pp. 221–228. [CrossRef]
58. Carter, R.W.G. *Coastal Environments: An Introduction to the Physical, Ecological and Cultural Systems of Coastlines*; Academic Press Inc.: Cambridge, MA, USA, 1988; ISBN 0121618552.
59. Taylor, J.A.; Murdock, A.P.; Pontee, N.I. A macroscale analysis of coastal steepening around the coast of England and Wales. *Geogr. J.* **2004**, *170*, 179–188. [CrossRef]

60. Dornbusch, U.; Williams, R.B.G.; Moses, C.A.; Robinson, D.A. Foreshore narrowing along the coast of southeast England, UK—A reevaluation. *J. Coast. Res.* **2008**, *24*, 14–24. [CrossRef]
61. Orford, J.; Anthony, E. 10.9 Coastal Gravel Systems. In *Treatise on Geomorphology*; Elsevier: Amsterdam, The Netherlands, 2013; pp. 245–266.
62. Simeone, S.; Palombo, L.; De Falco, G. Morphodynamics of a nontidal embayed beach: The case study of is arutas (Western Mediterranean). *J. Coast. Res.* **2013**, *29*, 63–71. [CrossRef]
63. Alexandrakis, G.; Ghionis, G.; Poulos, S. The Effect of Beach Rock Formation on the Morphological Evolution of a Beach. The Case Study of an Eastern Mediterranean Beach: Ammoudara, Greece. *J. Coast. Res.* **2013**, *69*, 47–59. [CrossRef]
64. Bascom, W.N. The relationship between sand size and beach-face slope. *Trans. Am. Geophys. Union* **1951**, *32*, 866. [CrossRef]
65. Wright, L.D.; Short, A.D. Morphodynamic variability of surf zones and beaches: A synthesis. *Mar. Geol.* **1984**, *56*, 93–118. [CrossRef]
66. Ranasinghe, R.; McLoughlin, R.; Short, A.; Symonds, G. The Southern Oscillation Index, wave climate, and beach rotation. *Mar. Geol.* **2004**, *204*, 273–287. [CrossRef]
67. Thomas, T.; Phillips, M.R.; Williams, A.T.; Jenkins, R.E. Medium time-scale behaviour of adjacent embayed beaches: Influence of low energy external forcing. *Appl. Geogr.* **2012**, *32*, 265–280. [CrossRef]
68. Short, A.D.; Trembanis, A.C. Decadal scale patterns in beach oscillation and rotation Narrabeen beach, Australia—Time series, PCA and wavelet analysis. *J. Coast. Res.* **2004**, *20*, 523–532. [CrossRef]
69. Kuang, C.; Han, X.; Zhang, J.; Zou, Q.; Dong, B. Morphodynamic Evolution of a Nourished Beach with Artificial Sandbars: Field Observations and Numerical Modeling. *J. Mar. Sci. Eng.* **2021**, *9*, 245. [CrossRef]
70. Davidson-Arnott, R. 10.6 Nearshore Bars. In *Treatise on Geomorphology*; Shroder, J., Sherman, D.J., Eds.; Academic Press: San Diego, CA, USA, 2013; Volume 10, pp. 130–148. ISBN 9780080885223.
71. Oppenheimer, M.; Glavovic, B.C.; Hinkel, J.; van de Wal, R.; Magnan, A.K.; Abd-EIgawad, A.; Cai, R.; Cifuentes-Jara, M.; DeConto, R.M.; Ghosh, T.; et al. *Sea Level Rise and Implications for Low-Lying Islands, Coasts and Communities*; Pörtner, H.-O., Roberts, D.C., Masson-Delmotte, V., Zhai, P., Tignor, M., Poloczanska, E., Mintenbeck, K., Alegría, A., Nicolai, M., Okem, A., et al., Eds.; Cambridge University Press: Cambridge, UK; New York, NY, USA; Geneva, Switzerland, 2019; pp. 321–446. [CrossRef]
72. Evelpidou, N.; Petropoulos, A.; Karkani, A.; Saitis, G. Evidence of Coastal Changes in the West Coast of Naxos Island, Cyclades, Greece. *J. Mar. Sci. Eng.* **2021**, *9*, 1427. [CrossRef]
73. Karkani, A.; Evelpidou, N.; Giaime, M.; Marriner, N.; Morhange, C.; Spada, G. Late Holocene sea-level evolution of Paros Island (Cyclades, Greece). *Quat. Int.* **2019**, *500*, 139–146. [CrossRef]
74. Defeo, O.; McLachlan, A.; Schoeman, D.S.; Schlacher, T.A.; Dugan, J.; Jones, A.; Lastra, M.; Scapini, F. Threats to sandy beach ecosystems: A review. *Estuar. Coast. Shelf Sci.* **2009**, *81*, 1–12. [CrossRef]
75. Smith, K. We are seven billion. *Nat. Clim. Change* **2011**, *1*, 331–335. [CrossRef]
76. Brown, S.; Nicholls, R.J.; Goodwin, P.; Haigh, I.D.; Lincke, D.; Vafeidis, A.T.; Hinkel, J.; Brown, S.; Nicholls, R.J.; Goodwin, P.; et al. Quantifying Land and People Exposed to Sea-Level Rise with No Mitigation and 1.5 °C and 2.0 °C Rise in Global Temperatures to Year 2300. *EaFut* **2018**, *6*, 583–600. [CrossRef]
77. Orford, J.D.; Pethick, J. Challenging assumptions of future coastal habitat development around the UK. *Earth Surf. Processes Landf.* **2006**, *31*, 1625–1642. [CrossRef]
78. WHO. *COP24 Special Report: Health and Climate Change*; World Health Organization: Geneva, Switzerland, 2018.
79. IPCC. *Global Warming of 1.5 °C The Context Of Strengthening The Global Response To The Threat Of Climate Change, Sustainable Development, and Efforts to Eradicate Poverty*; IPCC: Geneva, Switzerland, 2018.
80. Norwegian Red Cross (NRC). *Overlapping Vulnerabilities: The Impacts of Climate Change on Humanitarian Needs*; Norwegian Red Cross: Oslo, Norway, 2019.
81. Chapin, F.S.; Carpenter, S.R.; Kofinas, G.P.; Folke, C.; Abel, N.; Clark, W.C.; Olsson, P.; Smith, D.M.S.; Walker, B.; Young, O.R.; et al. Ecosystem stewardship: Sustainability strategies for a rapidly changing planet. *Trends Ecol. Evol.* **2010**, *25*, 241–249. [CrossRef]
82. Cantasano, N.; Pellicone, G.; Ietto, F. The Coastal Sustainability Standard method: A case study in Calabria (Southern Italy). *Ocean. Coast. Manag.* **2020**, *183*, 104962. [CrossRef]
83. Del-Rosal-Salido, J.; Folgueras, P.; Bermúdez, M.; Ortega-Sánchez, M.; Losada, M. Flood management challenges in transitional environments: Assessing the effects of sea-level rise on compound flooding in the 21st century. *Coast. Eng.* **2021**, *167*, 103872. [CrossRef]